RUTHENIUM(0) NANOPARTICLES SUPPORTED ON GRAPHENE:
PREPARATION, CHARACTERIZATION AND CATALYTIC USE IN HYDROGEN
GENERATION FROM HYDROLYSIS OF AMMONIA BORANE

A THESIS SUBMITTED TO
THE GRADUATE SCHOOL OF NATURAL AND APPLIED SCIENCES
OF
MIDDLE EAST TECHNICAL UNIVERSITY

BY

FATMA ASİYE ACAR

IN PARTIAL FULFILLMENT OF THE REQUIREMENTS
FOR
THE DEGREE OF MASTER OF SCIENCE
IN
CHEMISTRY

JANUARY 2015

Approval of the Thesis:

RUTHENIUM(0) NANOPARTICLES SUPPORTED ON GRAPHENE: PREPARATION, CHARACTERIZATION AND CATALYTIC USE IN HYDROGEN GENERATION FROM HYDROLYSIS OF AMMONIA BORANE

submitted by **FATMA ASİYE ACAR** in partial fulfillment of the requirements for the degree of **Master of Science in Chemistry Department, Middle East Technical University** by,

Prof. Dr. Gülbin Dural Ünver   _____
Dean, Graduate School of **Natural and Applied Sciences**

Prof. Dr. İlker Özkan   _____
Head of Department, **Chemistry**

Prof. Dr. Saim Özkâr   _____
Supervisor, **Chemistry Department, METU**

Examining Committee Members:

Prof. Dr. Ceyhan Kayran   _____
Chemistry Dept., METU

Prof. Dr. Saim Özkâr   _____
Chemistry Dept., METU

Prof. Dr. İzzet Morkan   _____
Chemistry Dept., Abant İzzet Baysal University

Assoc. Prof. Dr. Ayşen Yılmaz   _____
Chemistry Dept., METU

Assoc. Prof. Dr. Emren Nalbant Esentürk   _____
Chemistry Dept., METU

Date: _____05.01.2015_____

Name, Last Name: Fatma Asiye Acar

Signature   :

ABSTRACT

RUTHENIUM(0) NANOPARTICLES SUPPORTED ON GRAPHENE: PREPARATION, CHARACTERIZATION AND CATALYTIC USE IN HYDROGEN GENERATION FROM HYDROLYSIS OF AMMONIA BORANE

Acar, Fatma Asiye

M. S., Department of Chemistry

Supervisor: Prof. Dr. Saim Özkâr

January 2015, 96 pages

The development of new storage materials will facilitate the use of hydrogen as a major energy carrier in near future. In hydrogen economy, chemical hydrides have been tested as hydrogen storage materials for supplying hydrogen at ambient temperature. Among these chemical materials, ammonia borane having a high content of hydrogen (19.6 wt.%) seems to be an ideal hydrogen storage material since it is stable under ordinary conditions and releases hydrogen gas in a safe and controllable way in aqueous solutions. However, hydrolysis of ammonia borane requires a suitable catalyst. In this thesis, the preparation, characterization and investigation of the catalytic activity of the ruthenium(0) nanoparticles supported on graphene were reported.

In order to obtain ruthenium(0) nanoparticles supported on graphene, first graphene oxide was prepared from graphite by using modified Hummers' method. Then Ru^{3+} ions were impregnated onto graphene oxide. Finally, ammonia borane was used to reduce ruthenium(III) ions to ruthenium(0) nanoparticles supported on graphene. The ruthenium(0) nanoparticles were characterized by ICP-OES, XRD, SEM, SEM/EDX and TEM. Ruthenium(0) nanoparticles supported on graphene were used to catalyze the hydrolysis of ammonia borane releasing 3 equivalent of hydrogen per mole of ammonia borane. They are highly active catalyst providing 200,000 turnovers in hydrogen generation from the hydrolysis of ammonia borane at 25.0 ± 0.1 °C with an initial turnover frequency value of 150 min^{-1}. The kinetics of the catalytic hydrolysis of ammonia borane was studied depending on the catalyst concentration, substrate concentration, and temperature. The kinetic study shows that the ruthenium(0) nanoparticles-catalyzed hydrolysis of ammonia borane is first order with respect to catalyst concentration and zero order with respect to substrate concentration. The activation parameters of this reaction were determined from the evaluation of the kinetic data.

Keywords: Ruthenium(0) nanoparticles; Hydrolysis; Ammonia borane; Heterogeneous catalyst; Graphene; Hydrogen generation.

ÖZ

GRAFEN ÜZERİNDE DESTEKLENDİRİLMİŞ RUTENYUM(0) NANOPARÇACIKLARI:
HAZIRLANMASI, KARAKTERİZASYONU VE AMONYAK BORAN HİDROLİZİNDEN HİDROJEN ÜRETİMİNDE KATALİTİK OLARAK KULLANILMASI

Acar, Fatma Asiye

Y. Lisans, Kimya Bölümü

Tez Yöneticisi: Prof. Dr. Saim Özkâr

Ocak 2015, 96 sayfa

Yakın gelecekte, depolama tekniklerinin gelişimi ile hidrojenin enerji taşıyıcı olarak kullanılması büyük ölçüde kolaylaşacaktır. Hidrojen ekonomisinde, istenilen sıcaklıkta hidrojen eldesi için, kimyasal hidrürler hidrojen depolama malzemesi olarak test edilmektedir. Bu kimyasallar arasında, normal koşullarda kararlı yapıda olması, sulu çözeltisinde güvenli ve kontrollü bir şekilde hidrojen gazı elde edilmesi sebebiyle yüksek bir hidrojen konsantrasyonuna (%19.6) sahip olan amonyak boranı ideal bir hidrojen depolama malzemesi haline getirmektedir. Fakat amonyak borandan hidrojen eldesi uygun bir katalizör kullanımı gerektirmektedir. Bu çalışmada, grafen üzerinde

desteklendirilmiş rutenyum(0) nanoparçacıklarının hazırlanması, karakterizasyonu ve amonyak boran hidrolizinden hidrojen üretiminde katalitik olarak kullanılması açıklanılmıştır.

Grafen üzerinde desteklendirilmiş rutenyum(0) nanoparçacıklarının elde edilebilmesi amacıyla ilk basamakta grafitten uyarlanmış Hummers yöntemi ile grafen oksit elde edildi. Daha sonra Ru^{3+} iyonları grafen oksitin içine yedirilmiş ve bu amonyak boran yardımıyla grafen üzerinde desteklendirilmiş rutenyum(0) nanoparçacıklarına indirgendi. Rutenyum(0) nanoparçacıklarının karakterisyonu Toz XRD, SEM, TEM, EDX ve ICP-OES spektroskopik yöntemleri ile elde edildi. Amonyak boranın rutenyum(0) nanoparçacıkları ile katalitik hidrolizi sulu çözelti içerisinde gerçekleştirildi ve tepkime kinetiği, katalizör derişimine, substrat derişimine, sıcaklığa bağlı olarak incelendi. Kinetik çalışmalar sonucunda rutenyum(0) nanoparçacıkları ile katalizlenen amonyak boranın hidrolizi tepkimesinin katalizör derişimine göre birinci dereceden ve substrat derişimine göre sıfırıncı dereceden olduğu bulundu. Kinetik verilerin değerlendirilmesi ile rutenyum(0) nanoparçacıkları ile katalizlenen amonyak boranın hidrolizi tepkimesinin aktivasyon parametreleri de belirlendi.

Anahtar Kelimeler: Rutenyum(0) nanoparçacıkları, amonyak boranın hidrolizi, heterojen katalizör, grafen.

To My Family

ACKNOWLEDGMENTS

TABLE OF CONTENTS

LIST OF TABLES

TABLES

LIST OF FIGURES

FIGURES

NOMENCLATURE

°C	Centigrade Degree
A	Pre-Exponential Factor
Å	Angstrom
Aq	Aqua
DNA	Deoxyribonucleic Acid
E_a	Energy of Activation
G	Gas
G	Graphene
GO	Graphene Oxide
H	Planck's Constant
HAp	Hydroxyapatite
K	Kelvin
K	Rate Constant
Kb	Boltzmann Constant
Kg	Kilogram
kJ	Kilojoule
L	Liquid
M	Meter
M	Molar
mg	Milligram
mL	Milliliter
mM	Millimolar
MWCNT	Multi-Walled Carbon Nanotube

P	Pressure
PSSA-co-MA	Poly(4-Styrene Sulfonicacid-Co-Maleic Acid)
R	Gas Constant
T	Temperature
X-NW	Xonotlite Nanowire
ZK-4	Zeolite
$\Delta H^{\ddagger}$	Enthalpy of Activation
$\Delta S^{\ddagger}$	Entropy of Activation
Θ	Theta
Mm	Micrometer
ρ_m	Gravimetric Density
ρ_v	Volumetric Density

ABBREVIATIONS

0D	Zero-Dimensional
1D	One-Dimensional
2D	Two-Dimensional
3D	Three-Dimensional
AB	Ammonia Borane
AFM	Atomic Force Microscopy
CVD	Chemical Vapor Deposition
DLVO	Derjaugin, Landau, Verwey, and Overbeek
EDS	Energy Dispersive Spectroscopy
EXAFS	Extended X-Ray Absorption Fine Structure
HPLC	High Performance Liquid Chromatography
HR-TEM	High Resolution Transmission Electron Microscopy
ICP-OES	Inductively Coupled Plasma Optical Emission Spectroscopy
IR	Infrared Spectroscopy
NIH	National Institutes of Health
NMR	Nuclear Magnetic Resonance Spectroscopy
NP	Nanoparticle
P-XRD	Powder X-Ray Diffraction
SEM	Scanning Electron Microscope
SEM/EDX	Scanning Electron Microscope Electron Diffraction X-Ray
STM	Scanning Tunneling Microscopy
TEM	Transmission Electron Microscopy
TOF	Turnover Frequency

TON	Turnover Number
TTON	Total Turnover Number
UV–Vis	Ultraviolet–Visible Spectroscopy
XRD	X-Ray Diffraction

CHAPTER 1

INTRODUCTION

Natural processes led to spontaneous accumulation of carbon based energy sources, so called fossil fuels, which have been used to meet around 80% of the world energy demand [1]. However, fossil fuels (i.e., petroleum, natural gas, and coal) are projected to be overused due to the increasing worldwide energy requirement which spells shortage of these resources in the next few decades [2]. The use of renewable energy sources namely, solar energy, wind power, hydro power, biomass energy, geothermal energy, tidal energy and wave power technologies are sought because of increasing concern about the environmental problems, including global warming caused by the emission of gases from the combustion of fossil fuels which is correlated with a number of casualties in warm climate countries, increasing levels of sea water worldwide which threatens seaside cities, and numerous other natural disasters such as floods, hurricanes, forest fires, and so on. [3,4]. The renewable energy sources, however, carry disadvantages such as relatively high cost, low efficiency, discontinuity, storage and transportation such as in solar and wind energy which are not always available. Significant amount of energy is lost while being stored or moved long distances. Therefore there is a need of an energy carrier for all of these energy sources, of which one is hydrogen. Alternatively being a clean and renewable energy carrier, hydrogen is widely available from diverse sources, such as clean-coal technology, biomass, water electrolysis, photoelectrochemical and photochemical water splitting and nuclear energy [3,5]. Hydrogen has found an increasing demand in industrial applications in the last

decades since the combination of molecular hydrogen and oxygen in a fuel cell generates electricity and heat whose only by-product is water while burning of fossil fuels generates CO_2 and a variety of pollutants [3,6,7]. In most part, hydrogen is used as a feedstock in the chemical and petrochemical industry, to produce principally ammonia, refined fossil fuels by hydrocracking, and a variety of chemicals. Hydrogen can also be used as a propellant for rockets and space shuttles and it is considered as a fuel for many hydrogen powered vehicles including more than 70 types of cars and trucks as well as dozens of buses [3]. Since hydrogen is gaseous up to extreme conditions, has very low gas density and high flammability, the storage proves to be a problem [3,8]. In this context, safe, reliable, compact, and cost-effective storage becomes a primary challenge for hydrogen storage technologies [9]. Current on-board hydrogen storage approaches include compressed hydrogen gas, cryogenic and liquid hydrogen, metal hydrides, high surface area sorbents (such as carbon based nanostructured materials), and chemical hydrogen storage [9,10]. Chemical hydrogen storage has been of particular interest, especially owing to the high hydrogen contents of the materials considered. Hydrogen containing compounds, especially boron hydrides, have been investigated for solid state hydrogen storage materials because of their relatively high volumetric and gravimetric hydrogen density [8,9]. Among boron hydrides, ammonia borane (H_3NBH_3, AB) has recently been attracting a great deal of attention as a hydrogen storage material due to its high hydrogen content (19.6 wt %), stability and safety under fuel cell operating conditions [11,12]. Only in the presence of suitable catalysts, ammonia borane releases hydrogen upon hydrolysis in aqueous solution according to Eq. 1.1. The reaction is exothermic with a standard enthalpy change of −156 kJ/mol at 25 °C [13].

$$NH_3BH_3(aq) + H_2O(l) \xrightarrow{catalyst} NH_4BO_2(aq) + 3H_2(g) \qquad (1.1)$$

Many catalyst systems including transition metals and their alloys have been tested for hydrogen generation from the hydrolysis of ammonia borane; however, the idea of using such a process with the clear aim of releasing hydrogen was first introduced by Chandra and Xu in 2006 [14,15]. Their studies have shown that adding catalytic amount of a suitable metal catalyst into the solutions with various concentrations leads to a release of hydrogen gas with an H_2 to NH_3BH_3 mole ratio up to 3.0, corresponding to 8.9 wt% of the starting materials NH_3BH_3 and H_2O [16]. Then, the same group has also reported the catalytic activities of non-noble metal catalyst (Co, Cu, Fe, Ni) supported on γ-Al_2O_3, SiO_2 and C in hydrogen generation from the hydrolysis of ammonia borane where the highest activity has been observed with Co/C while Fe containing catalyst showed no activity [17]. Relatively faster hydrogen generation was achieved in the presence of noble metal catalysts such as Pt, Rh and Ru at room temperature [18,19]. However, the high reactivity of nanoparticles causes the tendency toward the aggregation of nanoparticles and consequent decline in catalytic activity. The aggregation between nanoparticles can be prevented by using a stabilizer. A variety of stabilizers have been reported for catalysts providing electrostatic, steric, and electrosteric stabilization [20]. Another way is to use supporting materials which temporarily acquires stability upon aggregation between nanoparticles. Unique electrical and chemical properties of graphene, a Nobel Prize winning discovery, make it a valuable supporting material for the stabilization of metal nanoparticles [21].

Herein, the synthesis and characterization of ruthenium(0) nanoparticles supported on graphene as a catalyst in hydrogen generation from the hydrolysis of ammonia borane is presented. The ruthenium(0) nanoparticles supported on graphene were characterized by ICP-OES, XRD, SEM, SEM/EDX and TEM. The results reveal the formation of well-dispersed ruthenium(0) nanoparticles supported on graphene. The kinetics of the reaction was studied depending on the catalyst concentration, substrate concentration

3

and the temperature. The rate law of the catalytic reaction, activation energy and activation parameters of catalytic hydrolysis reaction were acquired through a kinetic study of the ruthenium(0) nanoparticles supported on graphene catalyzed hydrolysis of ammonia borane.

The synthesis of ruthenium nanoparticles supported on graphene and the kinetic studies concerning hydrogen generation from catalytic hydrolysis of ammonia borane has been the subject of a publication during this thesis [22]. While it covers the synthesis of ruthenium nanoparticles supported on graphene via a one-step procedure using methylamine borane as reducing agent and the kinetics of the catalytic reaction, herein the synthesis of ruthenium nanoparticles supported on graphene by using ammonia borane, the kinetic studies and the catalytic lifetime of the catalyst were further elaborated; therefore the literature is remedied for points that are missing explanation.

CHAPTER 2

LITERATURE REVIEW

2.1. Hydrogen

2.1.1. Global Energy Problems

As a consequence of excessive fossil fuel consumption, large amounts of greenhouse gases, along with other toxic products, are released to the atmosphere causing global climate change and planet wide pollution [3]. Decrease of fossil fuel sources also has the potential to trigger a chain of events that will eventually incite world conflict, which are listed in Figure 2.1:
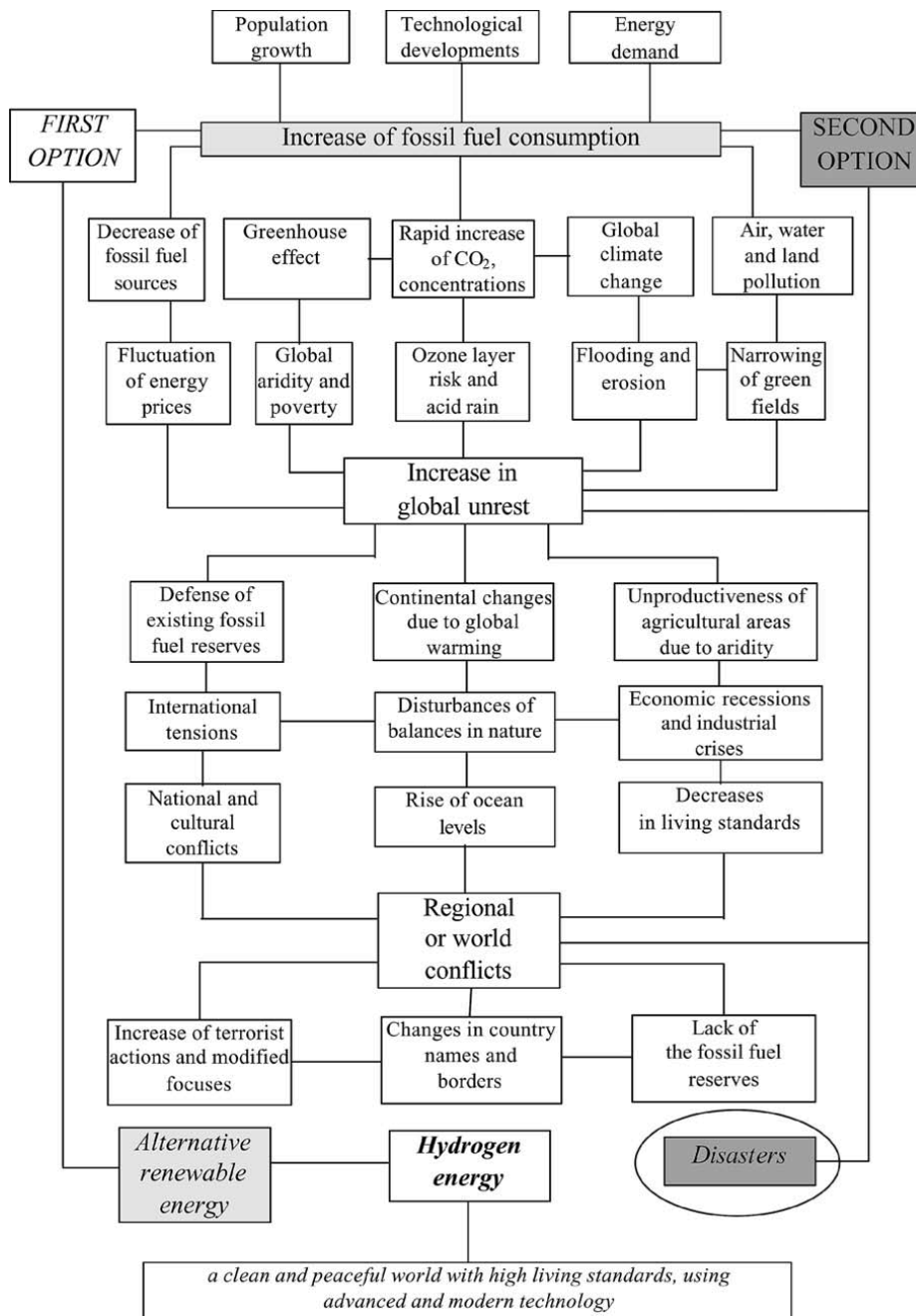
Figure 2.1. Possible global problems from increasing use of fossil fuels and the consequent need for hydrogen energy systems [2].

For centuries, fossil energy sources have met energy demands; however, due to the rapid increase in world population and finite amount of fossil energy sources, they will not be able to hold their place as primary energy sources [2,4]. The usage of fossil fuel types has shifted significantly over the last 90 years. In 1925, 80% of the required energy was supplied from coal while in the past few decades, 45% came from petroleum, 25% from natural gas and 30% from coal. Energy experts point out that reserves are less than 40 years for petroleum, 60 years for natural gas and 250 years for coal [10]. This will result in an increase of fossil fuels costs leading to obligatory pursuit of alternative fuels such as solar, wind, hydrogen related sources. As an example, observed and projected quantities of world energy production and consumption from 1971 to 2040 are displayed in Figure 2.2. [1]:
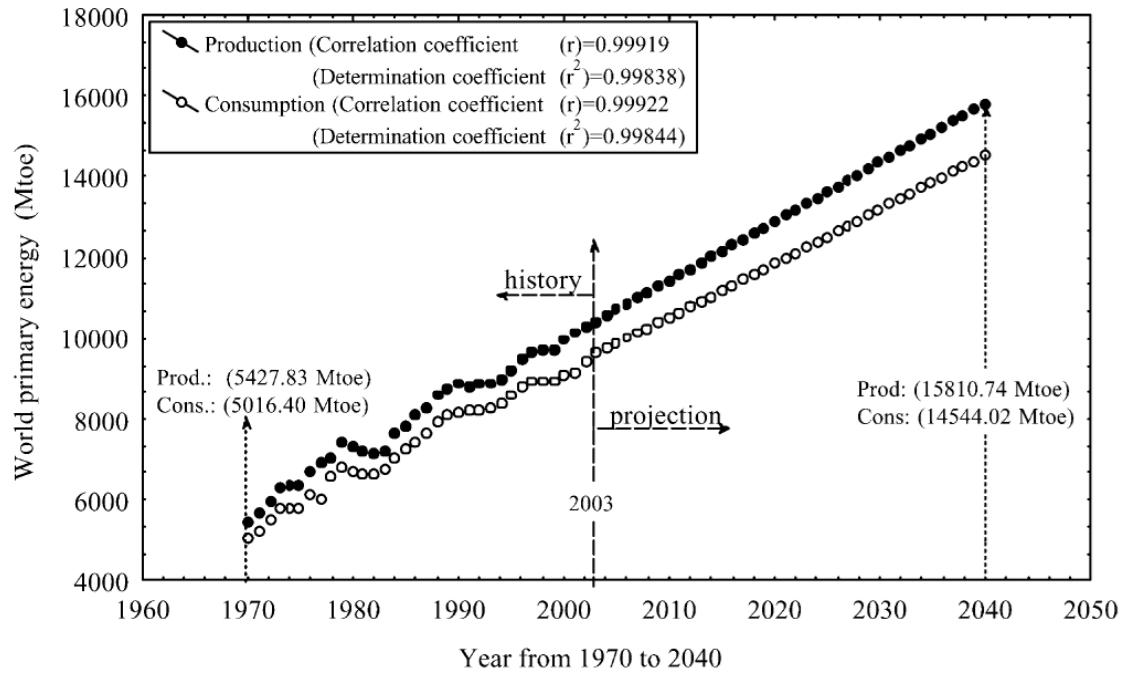
Figure 2.2. Variation of world energy production and consumption [1].

2.1.2. Hydrogen as an Energy Carrier

Hydrogen is expected to play an important role in future energy scenarios. The foremost factor that will determine the specific role of hydrogen will likely be energy demand. In the future, hydrogen is expected to replace fossil fuels to some degree and to become the preferred portable energy carrier for vehicles [6].

Hydrogen is a non-toxic, clean energy carrier that has a high specific energy on a mass basis. It can be produced from various processes [5] including use of solar and

8

renewable energy sources, fossil fuels (e.g., steam reforming of natural gas or other light hydrocarbons, gasification of coal and other heavy hydrocarbons), electrolysis of water, direct and indirect thermochemical decomposition. It can be stored over relatively long periods of time and has more usage area compared to electricity as shown in the Figure 2.3. It does not produce toxic exhaust emissions, except at some equivalence ratios (where its high flame temperature can result in significant levels of NO_x in the exhaust products) when combusted [23].
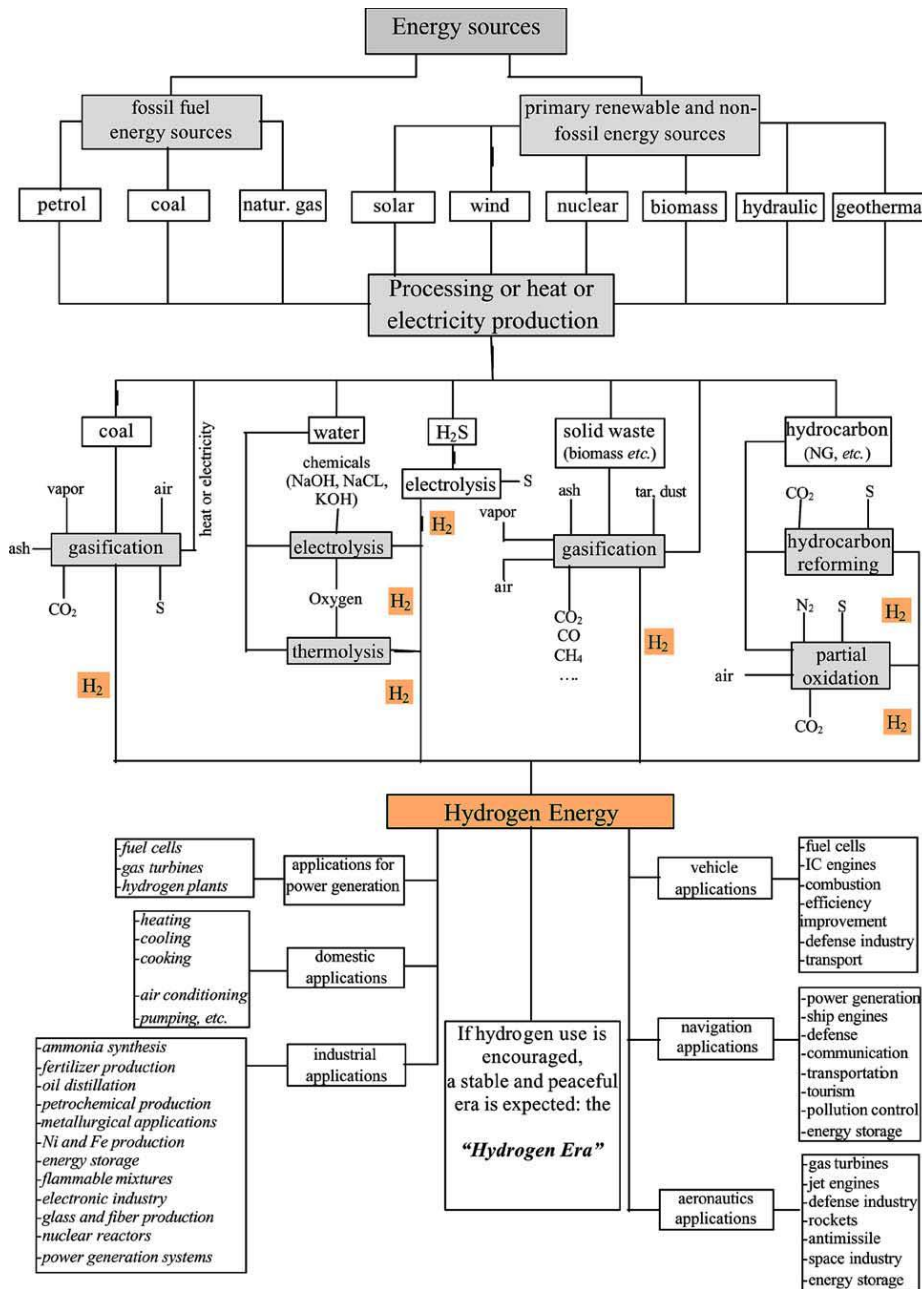
Figure 2.3. Relationship of production techniques and types of utilization of hydrogen [2].

10

However, as it is illustrated in the Table 2.1, hydrogen is highly inflammable when mixed with air, it can burn in lower concentrations which may cause safety concerns and storage of hydrogen in liquid form is difficult, as very low temperatures are required to liquefy hydrogen.

Table 2.1. The properties of hydrogen compared to the other fuels [3,24].

	Hydrogen	Gasoline	Methanol	Methane	Propane	Ammonia
Boiling Point [K]	20.3	350-400	337	112	231	240
Liquid density [kg m^{-3}]	71	702	797	425	507	771
Gas density [kg m^{-3}]	0.08	4.68	-	0.66	1.87	0.69
Lower heating value (mass) [MJ kg^{-1}]	120.0	44.4	20.1	50.0	46.4	18.6
Lower heating value (liquid) [MJ m^{-3}]	8960	31170	16020	21250	23520	14350
Lower Flammability limit [vol, % in air]	4	1	7	5	2	15
Lower Flammability limit (at 0 °C, 1 atm) [vol, % in air]	75	6	36	15	10	28

2.1.3. Hydrogen Storage

Hydrogen exhibits the highest heating value per mass of all chemical fuels. Furthermore, hydrogen is regenerative and environmentally friendly. There are two reasons why hydrogen is not the major fuel of today's energy consumption. First of all, hydrogen is not an energy source but indeed an energy carrier. Although it is the most abundant element in the universe, it only occurs in the form of water and hydrocarbons on Earth. The necessity to extract hydrogen first results in a difficult economic dilemma. The second difficulty with hydrogen as an energy carrier is its low critical temperature of 33 K (i.e. hydrogen is a gas at ambient temperature) [8]. For mobile and stationary applications the volumetric and gravimetric density of hydrogen in a storage material is crucial. Hydrogen can be stored using six different methods as listed in the Table 2.2:

Table 2.2. The six basic hydrogen storage methods [8].

Storage Method	ρ_m [mass %][a]	ρ_v [kg H_2 m^{-3}][b]	T [°C][c]	P [bar][d]
High pressure gas cylinders	13	<40	RT[e]	800
Liquid hydrogen in cryogenic tanks	size dependent	70.8	-252	1
Adsorbed hydrogen	≈ 2	20	-80	100
Absorbed on interstitial sites in a host metal	≈ 2	150	RT	1
Complex compounds	<18	150	>100	1
Metals and complexes together with water	<40	>150	RT	1

[a]Gravimetric density, [b]Volumetric density, [c]Operational temperature for storage method, and [d]Operational pressure for the storage method. [e]Room temperature (25°C).

Alongside well-established, high-pressure cylinders for laboratory applications and liquid hydrogen storage methods for air and space applications, metal hydrides and complex hydrides offer a safe and efficient way to store hydrogen. Further research and technical development will lead to higher volumetric and gravimetric hydrogen density [9,25]. Figure 2.4 shows the volumetric versus gravimetric hydrogen density for the various materials, in which it can be deduced that ammonia borane has a higher gravimetric density than most other reported chemical systems.

Ammonia borane (NH_3BH_3, AB), isoelectronic with ethane, is solid at room temperature, stable in air and water and has a high hydrogen storage capacity up to 19.6

wt.% (100–140 g/L) for release of three hydrogen molecules. There is an increasing demand on ammonia borane research as a hydrogen storage material, since it is stable and commercially available [26].
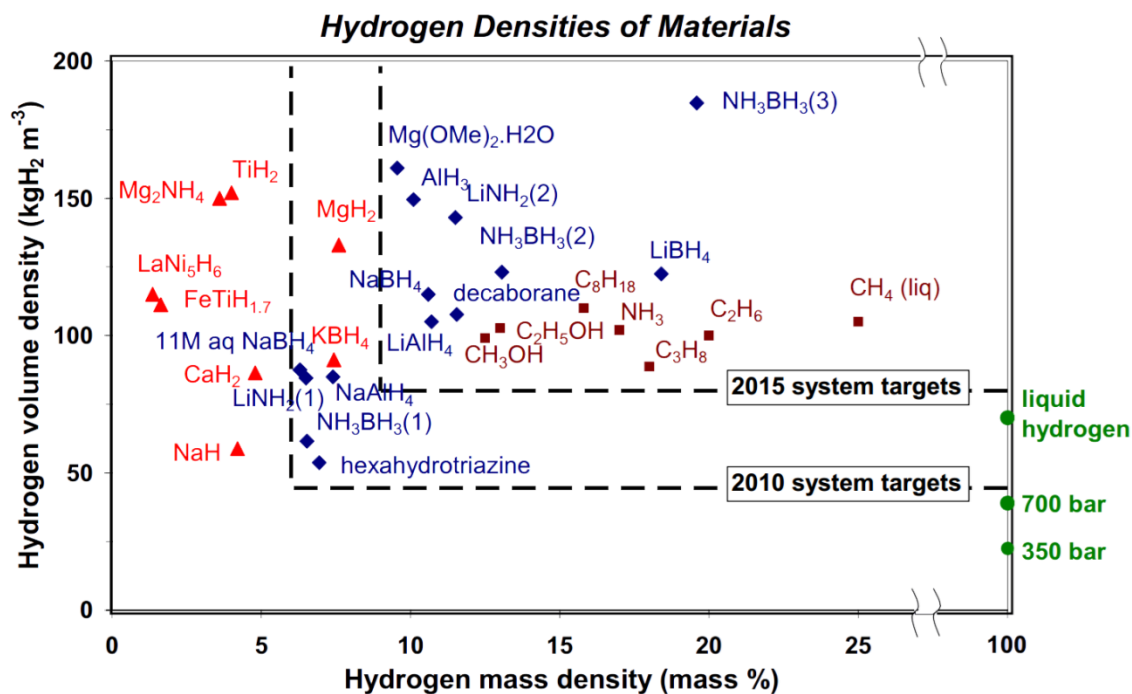
Figure 2.4. Representation of gravimetric and volumetric densities of different hydrogen storage materials [10].

At ambient temperature the structure of ammonia borane is tetragonal with a B–N distance as 1.56–1.58 Å which is unusually short for this type of electron donor–

14

acceptor compound [27]. A particularly important feature of AB materials is the existence of the so-called dihydrogen bond. Guided by the relatively short distance of 2.02 Å compared to the sum of the van der Waals radius of 2.4 Å between the nearest hydridic and protic hydrogen atoms located at the boron and nitrogen atom of different AB molecules, an unknown type of bond, the dihydrogen bond, was postulated [28,29]. The existence of the dihydrogen bond largely explains the very different melting points of BH_3NH_3 (110 °C) and the isoelectronic compound ethane (-182.77 °C) [29,30,31], as well as the higher volumetric hydrogen storage density of AB compared to ethane.

There are many different methods to obtain hydrogen from ammonia borane including dehydrogenation [32,33], thermolysis [34,35], and solvolysis (hydrolysis and methanolysis) [15,36]. Among them, the catalytic hydrolysis of AB appears to be the most convenient one for the storage of hydrogen [15,36]. As shown in the equation, it is suggested that hydrogen will be released a maximum of 9 wt.% with respect to the AB and to the consumed water weight [37]. Hydrolysis of AB in aqueous solution, results in producing gaseous hydrogen and ammonium metaborate (NH_4BO_2) with strong B−O bonds:

$$NH_3BH_3(aq) + H_2O(l) \xrightarrow{catalyst} NH_4BO_2(aq) + 3H_2(g) \qquad (2.1)$$

2.2. Transition Metal(0) Nanoclusters

2.2.1. Colloidal Metal Nanoclusters

Over the last decade there has been increased interest in "nanochemistry" [38]. *Nanoscience* is the technology development and research at the atomic, molecular or macromolecular levels, in the length scale of approximately $1 - 100$ nanometer range, to
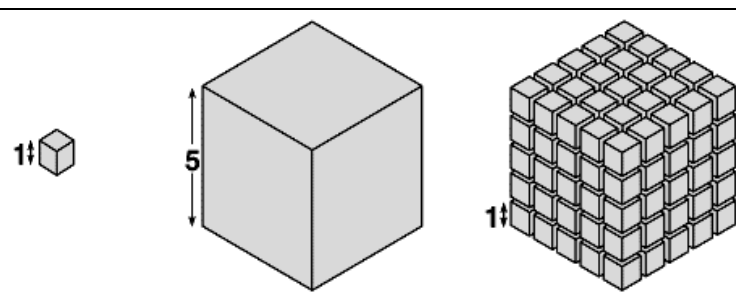
provide a fundamental understanding of phenomena and materials at the nanoscale and to create and use structures, devices and systems that have novel properties and functions because of their small and/or intermediate size. The novel and differentiating properties and functions are developed at a critical length scale of matter typically under 100 nm [39].

The term *nanotechnology* was introduced to describe physicist Richard Feynman's vision of factories using nanomachines to build complex products, including other nanomachines [40]. Engineering analysis indicates that this will be an extremely powerful capability, able to make large products with atomic precision, building them with superior materials, cleanly, and at low cost [41].

It is important to distinguish *modern nanoclusters* from at least *traditional colloids* or *nanoparticles* [42]. *Nanoclusters* are mono dispersed particles constituting an intermediate state of matter between molecules and solids about 1–10 nm (10–100 Å) in size [20] They are of considerable current interest, both fundamentally and for their possible applications in catalysis, in nano based chemical sensors [43], as light-emitting diodes [44], in "quantum computers" [45], or other molecular electronic devices [46,47],. Nanoclusters have been found to catalyze a range of reactions, spanning hydrogenations [48]; enantioselective hydrogenations [49]; hydrosilylations [50]; hydropyrolysis and hydrogenolysis [51]; oxidation of CO and CO/H_2 [52]; oxidative acetoxylation [53]; McMurry [54], Suzuki [55], and Heck-Type [56] couplings; and, most recently cycloaddition reactions [57]. Additional possible applications of nanoclusters are in ferrofluids for cell separations or in optical, electronic, or magnetic devices constructed via a building block, "bottom-up" approach [58,59,60]. *Nanoparticles* instead consist of up to a couple of hundred atoms, and larger aggregates containing 103 or more atoms [61].

Nanoclusters, have properties and structures which are very sensitive to their composition and size, which can lead to new and interesting properties not realized in the corresponding bulk material. Their physical and chemical properties gradually change from solid state to molecular behaviour with decreasing particle size [62]. When no other molecules are adsorbed onto the nanocrystallites, the surface atoms are highly unsaturated and their electronic contribution to the behaviour of the particles is totally different from that of the inner atoms. These effects may be even more marked when the surface atoms are ligated [63]. This leads to different mechanical and electronic transport properties, which account for the catalytic properties of the nanocrystalline particles [64]. As indicated in Table 2.3, the decrease in particle size results in the increase in the number of the atoms on surface thus enhancing the surface area while keeping the volume same.

Table 2.3. The effect of particle size on the ratio of the number of surface atoms to the total number of atoms.

Total surface area	6	150	750
Total volume	1	125	125
Surface to volume ratio	6	1.2	6

Especially for metal and semiconductor nanoparticles, the band structure gradually evolves with increasing particle size, i.e., molecular orbitals convert into delocalized band states. Figure 2.5 shows the size quantization effect responsible for the transition between a bulk metal or semiconductor, and cluster species. In a metal, the "quasi-continuous" density of states in the valence and the conduction bands splits into discrete electronic levels, the spacing between these levels and the band gap increasing with decreasing particle size [65, 66].
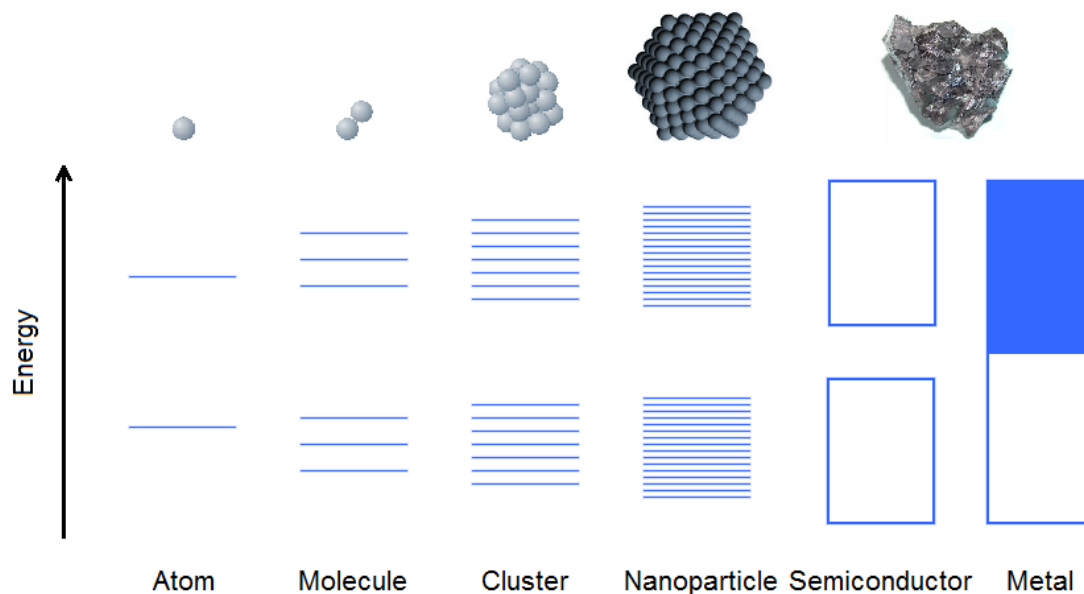
Figure 2.5. Size quantization effect. Electronic state transition from bulk metal/semiconductor to small cluster.

To investigate the physical and chemical properties of transition metal nanoparticles, a great degree of control over size, structure, and surface composition is essentially required.

2.2.2. Preparation of Transition Metal(0) Nanoparticles

Nanoparticles have been synthesized by a variety of methods [67]. Common synthetic techniques for semiconductor nanoparticles employ the use of constrained environments, such as inverse micelles [51,68,69]; capping agents, which arrest the growth of particles when they reach a certain size [70]; zeolites, ionomers, porous glass

[71] and gels [70]; solid polymer environments [72]; or dendrimers [73]. For transition metal nanoclusters; however, there are five general synthetic methods which are: (i) transition metal salt reduction, (ii) Thermal decomposition and photochemical methods, (iii) ligand reduction and displacement from organometallics, (iv) metal vapor synthesis [62], and (v) electrochemical synthesis [54].

2.2.3. Stabilization of Transition Metal(0) Nanoparticles

Nanoparticles are only kinetically stable; they must be stabilized against aggregation into larger particles and, eventually, bulk material, their thermodynamic minimum. Stabilization can be accomplished in three ways: electrostatic charge, or 'inorganic' stabilization, steric 'organic' stabilization or electrosteric stabilization combining both electrostatic and steric stabilization [20].

2.2.3.1. Electrostatic Stabilization

The classic theory of electrostatic colloidal stabilization was developed by Derjaugin, Landau, Verwey, and Overbeek, in the 1940s and is commonly referred to as DLVO theory [74]. DLVO theory predicts that nanocluster stabilization is based on a delicate balance in interparticle forces between repulsive Coulombic forces opposing attractive van der Waals forces. This theory is the most commonly used for the prediction of the so-called lyophobic colloid stability which is defined as having weak or no interactions between the colloid and the solvent [74]. Indeed, it was recently stated that "For colloid science the theory of DLVO stands at the same level of importance as does Darwin's theory of the origin of the species in Biology" [75].
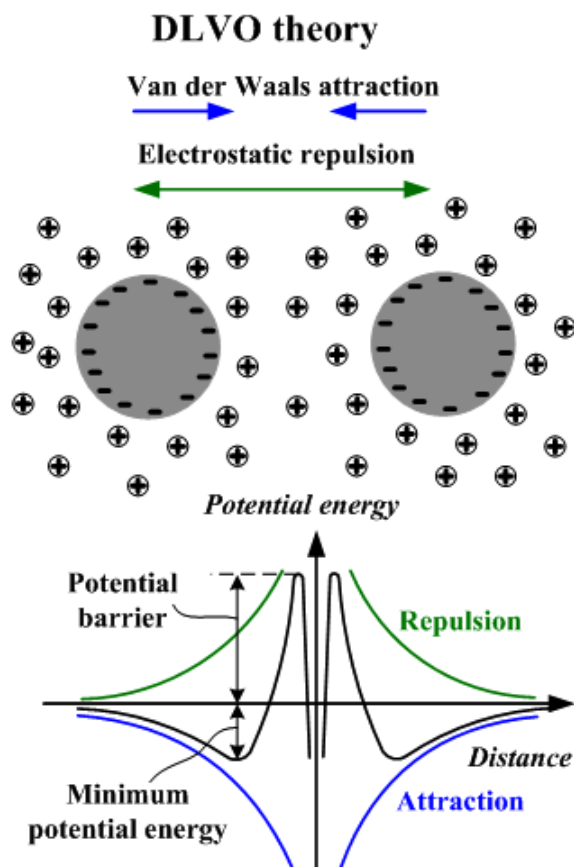
Figure 2.6. A schematic illustration for an electrostatically stabilized metal (M) particle (i.e., one stabilized by the adsorption of ions and the resultant electrical double layer) [20].

In DLVO-type electrostatic stabilization, the stabilizer of initial interest is the anion (Figure 2.6) [20]. Anions, whether added to the solution separately or present from reduction of a metal salt precursor, will be bound to any previously coordinatively unsaturated, electrophilic nanocluster surface [41]. Hence, anions form a layer

immediately adjacent to the nanocluster, providing the Columbic repulsion component of DLVO-type stabilization between two, now anionically charged particles. Counter cations are also present, to provide charge balance and complete the electronic multilayer. DLVO theory treats counterions as point charges, so small monoanions such as halides are among the closest "real-life", albeit still imperfect, examples of DLVO-type stabilization [76].

2.2.3.2. Steric Stabilization

Colloidal particles can be prevented from aggregating by the adsorption of molecules such as polymers, surfactants or ligands at the surface of the particles, thus providing a protective layer (Figure 2.7). Polymers are widely used, and the protectant must not only coordinate to the particle surface in order to function effectively, but must also be adequately solvated by the dispersing fluid-such polymers are termed amphiphilic. The choice of polymer is determined by consideration of the solubility of the metal colloid precursor, the solvent of choice, and the ability of the polymer to stabilize the reduced metal particles in the colloidal state [77].
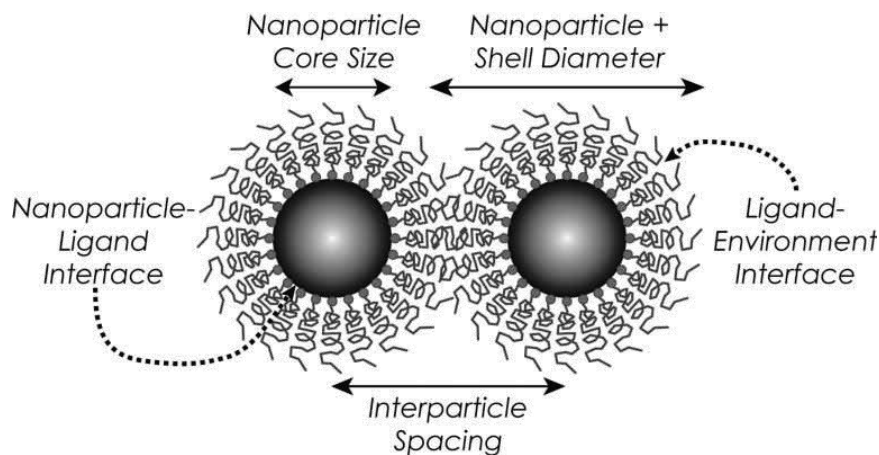
Figure 2.7. A schematic illustration for a sterically stabilized metal particle [78].

2.2.3.3. Electrosteric Stabilization

In the literature, many authors have combined the two well precedented modes of nanocluster stabilization into so-called "electrosteric" stabilization [79]. Tracking down the origin and a clear definition of this term proved difficult. As the term "electrosteric" implies, this mode of stabilization is a combination of electrostatic stabilization (as described in DLVO theory) and steric stabilization. Electrosteric stabilizers have the potential to be superior for catalytic applications, as the combination of electrostatic and steric stabilization may mean that fewer equivalents of stabilizer per nanocluster are necessary for stabilization, possibly leaving more coordinatively unsaturated surface atoms available for catalysis.

The first report on polyoxoanion-stabilized nanoclusters noted that the $P_2W_{15}Nb_3O_{62}^{9-}$ and associated $(Bu_4N)_9^{9+}$ stabilization of $Ir(0)_{\sim300}$ nanoclusters was of a novel type, a

"combined high charge plus significant steric bulk present intrinsically" [48] within the (ca. 15 Å by 12 Å [41]) polyoxoanion and nine Bu_4N^+ countercations. Since then, $P_2W_{15}Nb_3O_{62}{}^{9-}$ has been used to stabilize both Ir and Rh nanoclusters. Hence, it would be tempting to term these highly charged, sterically massive stabilizers as prototype "electrosteric" stabilizers.
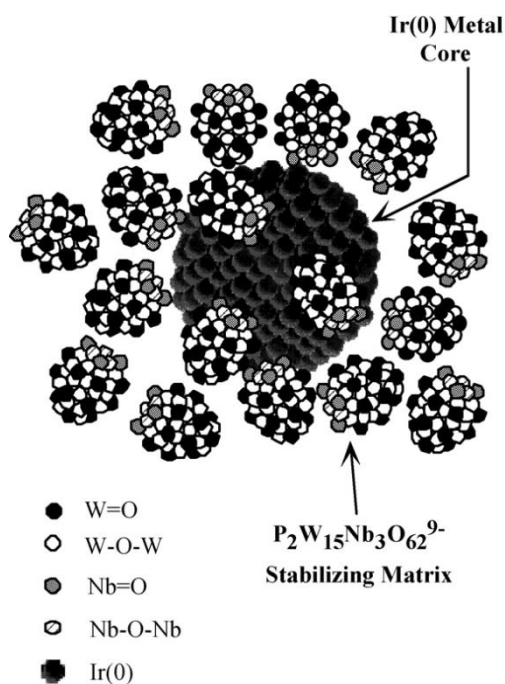
Figure 2.8. Idealized, roughly to scale representation of a $P_2W_{15}Nb_3O_{62}{}^{9-}$ polyoxoanion and Bu_4N^+ stabilized Ir(0)$_{\sim300}$ nanocluster [67].

2.2.4. Characterization of Transition Metal(0) Nanoparticles

Transmission Electron Microscopy (TEM), *UV–Visible Spectroscopy* (UV–Vis), *Nuclear Magnetic Resonance Spectroscopy* (NMR), *Infrared Spectroscopy* (IR), elemental analysis, and *Energy Dispersive Spectroscopy* (EDS), analytical ultracentrifugation–sedimentation, *Extended X-Ray Absorption Fine Structure* (EXAFS), *Scanning Tunneling Microscopy* (STM), *Atomic Force Microscopy* (AFM), *High Performance Liquid Chromatography* (HPLC), light scattering, time-of-flight mass spectrometry, magnetic susceptibility, and electrophoresis or ion-exchange chromatography are among the commonly preferred techniques for structural, compositional and topographic characterization of nanoparticles [20] (Figure 2.9).
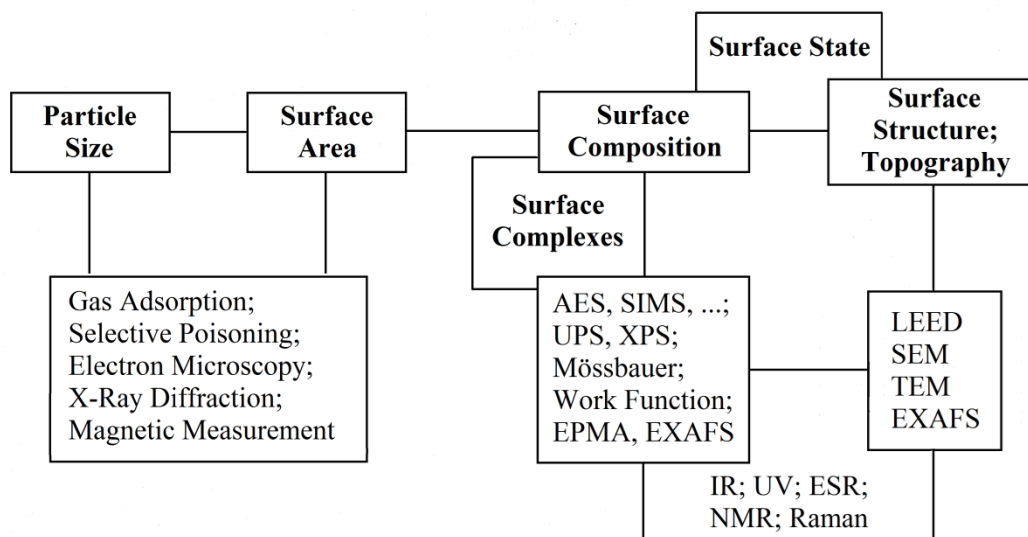
Figure 2.9. General view of methods available for the characterization of nanoparticles [80].

25

Transmission Electron Microscopy (TEM) and *High Resolution TEM* (HR-TEM) are widely used imaging methods, where interactions of an electron beam transmitted through an ultrathin surface characterize the size, shape, dispersity, structure, and morphology of nanoclusters [81].

In Scanning Electron Microscopy with Energy Dispersive X-Ray Spectroscopy (SEM/EDX), when inner shell electrons are ejected by an incident electron beam the atom becomes unstable and the resulting hole then is filled by an outer shell electron by emitting a photon. The energy difference between the shells usually falls into KeV region yielding X-rays [82].

In order to characterize semiconductor-type nanoparticles or metal particles whose plasmon resonance lies in the visible range, UV–Vis spectroscopy proves an effective method, which allows for determination of particle size along with aggregate analysis [83].

Infrared spectroscopy (IR) is often utilized as a surface probe in nanoparticle systems. Carbon monoxide adsorption onto the surface of a metal nanoparticle produces characteristic vibrational frequencies around 1800–2100 cm^{-1} thereby rendering CO a practical ligand in detection of surface properties of a nanoparticle [77].

Nuclear Magnetic Resonance (NMR) spectroscopy in nanoparticle studies, deals either with intra-core metallic atoms or the ligands that surround the metal core [84].

Scanning Tunneling Microscopy (STM) [61] makes possible the determination of the total diameter of a nanoparticle, including the stabilizing ligand shell. STM is also an effective probe of the electronic properties of such nanoparticles.

Atomic Force Microscopy (AFM) to image nanoparticles [85]. This technique, contrary to STM, is purely mechanical: a cantilevered tip attached to a spring is dragged across a sample. The increase or decrease in the height of the tip is measured, yielding a surface height profile as a function of distance.

2.3. Catalysis

2.3.1. General Principles of Catalysts

Almost all biochemical processes in nature, which are essential to life, such as the oxidation of sugar or DNA sequencing, are initiated and carried out by enzymes [86]. *Enzymes* can be defined as amino acid chains act as highly selective biological catalysts [87]. With the help of enzymes, the rates of most biochemical reactions which are inactive under the mild conditions of temperature and pressure, increases drastically by almost over a million-fold so reactions that would take years can be achieved in seconds. Biological systems have long inspired design principles of synthetic materials. Today up to 90% of chemical and refinery processes utilize the catalytic systems of biomimetic origin [88]. A *catalyst* is a substance that increases the rate of a chemical reaction without modifying the overall standard Gibbs energy change in the reaction. However, it can be recovered chemically unchanged at the end of the reaction since it is not consumed by the reaction. The phenomenon where a catalyst is used to speed or activate the system is called *catalysis* [89].

If only one phase is involved the catalysis can be classified as *homogeneous catalysis*; on the other hand if the reaction occurs at or near an interface between phases it is classified as *heterogeneous catalysis* [90].
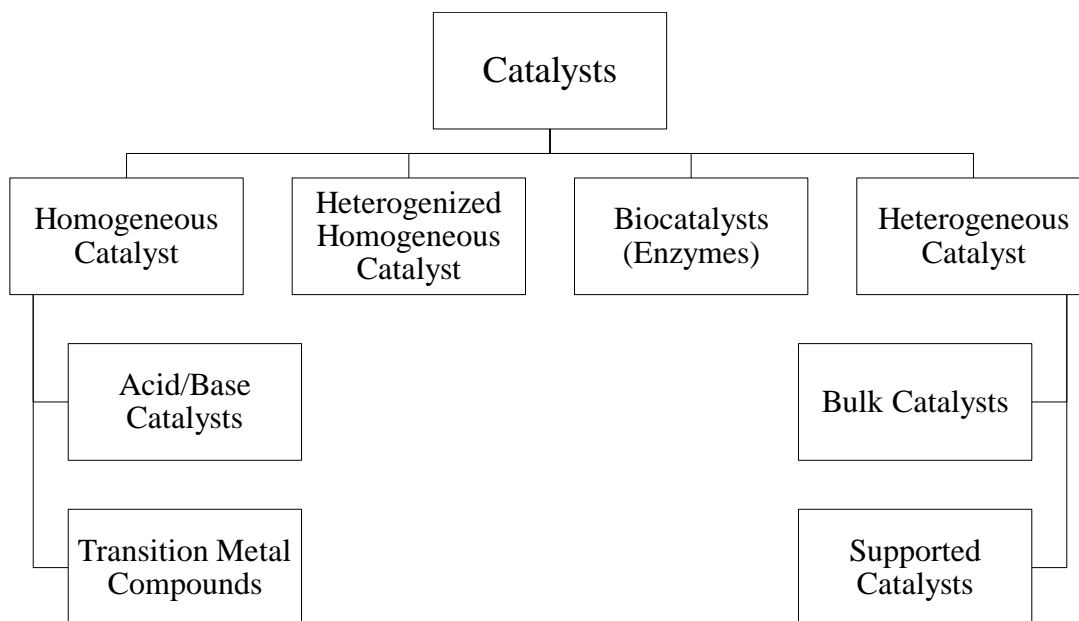
Figure 2.10. Classification of catalysts [91].

In any chemical reaction there is a need of rearrangement of chemical bonds. In *collision theory*, it is stated that the molecules react only if a collision occurs at energy equal to or greater than a certain critical value which is defined as the *energy of activation*, E_a [92]. In the *transition state theory*; however, products of the reaction can be formed if the molecules achieve a specific arrangement. The slowest step in the bond rearrangement having the highest enthalpy which is the *enthalpy of activation*, $\Delta H^{\ddagger}$, along the reaction coordinate is known as *transition state* [93]. The alternative route provided by the catalyst has a lower activation barrier than that of uncatalyzed reaction, allowing huge proportion of the reactants to attain needed energy to pass through the transition state and become products.

2.3.2. Energetics

When catalyst is used in a process, it affects the activation barriers of both forward and reverse reactions keeping the equilibrium position the same. In the case of synthesis of ammonia by Haber process, for instance;

$$N_2(g) + 3H_2(g) \rightleftarrows 2NH_3(g) \tag{2.2}$$
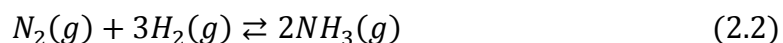
when catalyst not used, its activation energy is ca. 325 kJ mol^{-1} in the forward direction and 370 kJ mol^{-1} in the reverse direction. With addition of iron catalyst, the hydrogen and nitrogen molecules lose their translational degrees of freedom by attaching to the catalyst surface which reduces the activation energy dramatically and thus makes the energy of activation 103 kJ mol^{-1} for forward reaction [94]. The energy profiles for ammonia synthesis in the absence and presence of the catalyst is represented in Figure 2.11.
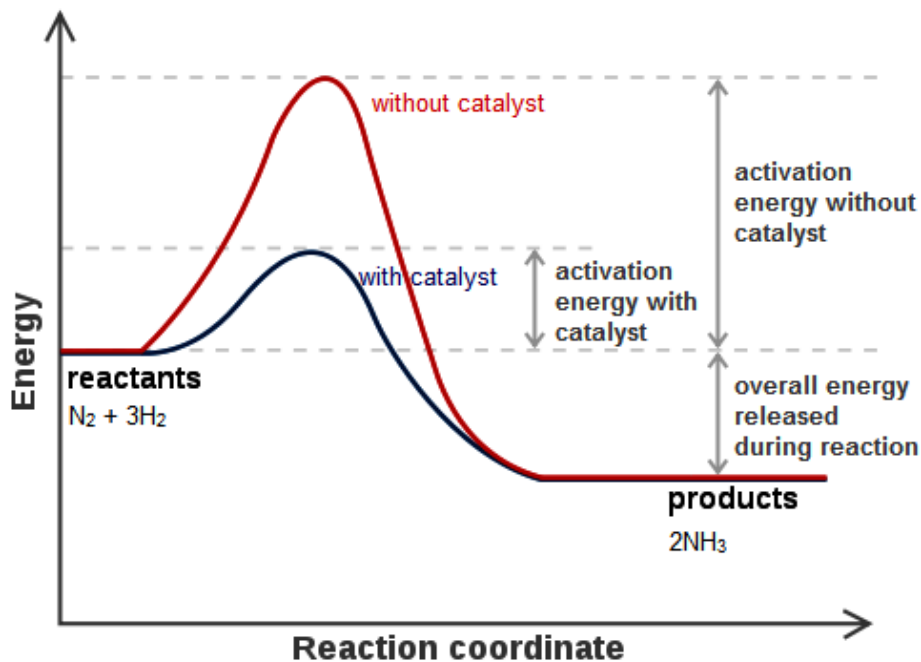
Figure 2.11. Effect of catalyst on the activation energy of the ammonia synthesis.

A catalyst alters the activation barrier in two ways either by binding to one or more of the reactants which reduces the energy needed by the reactant molecules in order to complete the reaction or bringing the reactants together and holding them tight so that the possibility of the reaction increases.

2.3.3. Properties of Catalysts

2.3.3.1. Catalytic Efficiency

In a catalytic process, first the catalyst should be in its active form in order to initiate or accelerate the reaction. Despite the numerous transformations a catalyst undergoes throughout a catalytic cycle, it prevails unchanged. An efficient catalyst can enter the cycle of states multiple times which can be named as the *turnover number*. The turnover number (TON) is the total number of reactant molecules that a catalyst converts into product molecules [91].

$$TON = \frac{volumetric\ rate\ of\ reaction}{number\ of\ centers/volume} . lifetime\ of\ the\ catalyst \quad (2.3)$$

The *turnover frequency* (TOF) quantifies the specific activity of a catalytic per unit time.

$$TOF = \frac{volumetric\ rate\ of\ reaction}{number\ of\ centers/volume} = \frac{moles}{volume.time}\frac{volume}{moles} = time^{-1} \quad (2.4)$$

2.3.3.2. Selectivity

The *selectivity* of a reaction is defined as the ratio of the starting material that is converted into the desired product. Therefore, a *selective* catalyst yields a high proportion of the desired product with minimum amount of the side products coming from parallel or sequential reactions [95]. Depending on the catalyst, same reactants yield different products, which have a large bearing in industrial catalysis.

31

$$\text{CO/H}_2 \begin{array}{l} \xrightarrow{\text{Ni}} \quad \text{CH}_4 + \text{H}_2\text{O} \qquad\qquad \text{Methanization} \\ \xrightarrow{\text{Cu/Cr/Zn Oxide}} \quad \text{CH}_3\text{OH} \qquad\qquad \text{Methanol Synthesis} \\ \xrightarrow{\text{Fe,Co}} \quad \text{C}_n\text{H}_{2n+m} + \text{H}_2\text{O} \qquad \text{Fischer} - \text{Tropsch Synthesis} \\ \xrightarrow{\text{Rh Cluster}} \quad \text{HO} - \text{CH}_2 - \text{CH}_2 - \text{OH} \quad \text{Glycol (Union Carbide)} \end{array}$$
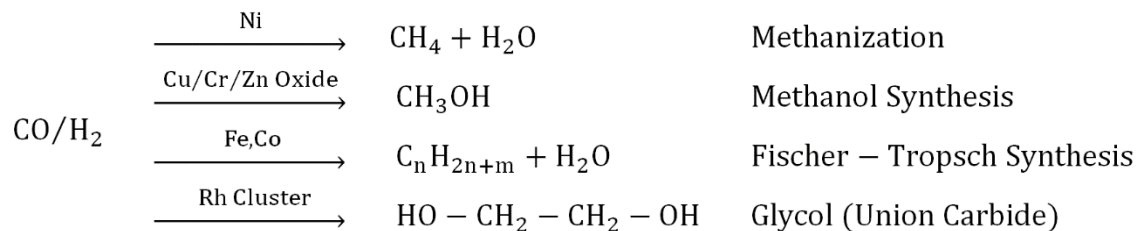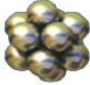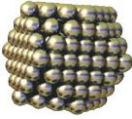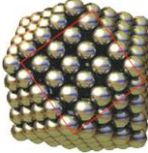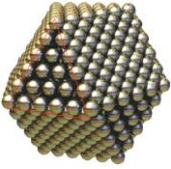
Figure 2.12. Various catalyst dependent routes for the reaction of CO and H_2 [95].

2.3.3.3. Importance of Size Reduction of Catalysts

The catalytic activity is a function of the surface area of a catalyst. Breaking down a bulky catalyst to smaller pieces increases its surface area, ensuring more active sites to react. As shown in Table 2.4 smaller particle size provides higher percentage of surface atoms which is directly proportional the activity of the catalyst [77,96].

32

Table 2.4. The relation between the total number of atoms in full-shell "magic number" clusters and the percentage of surface atoms.

Full-Shell "Magic Number" Clusters					
Number of Shells	1	2	3	4	5
Number of Atoms in Cluster	M_{13}	M_{55}	M_{147}	M_{309}	M_{661}
Percentage of Surface Atoms	92%	76%	63%	52%	45%

2.4. Graphene

Graphene is a flat monolayer of sp^2 hybridized carbon atoms tightly packed into a two-dimensional (2D) honeycomb lattice layer of the graphite structure with a C–C distance of 0.142 nm, having a nature of a polycyclic aromatic hydrocarbon of quasi infinite size [97]. For the graphite-like materials of all different dimensionalities (Figure 2.13), graphene can be used as a fundamental starting material by wrapping up into 0D fullerenes, rolling into 1D nanotubes or stacking into 3D graphite [98].
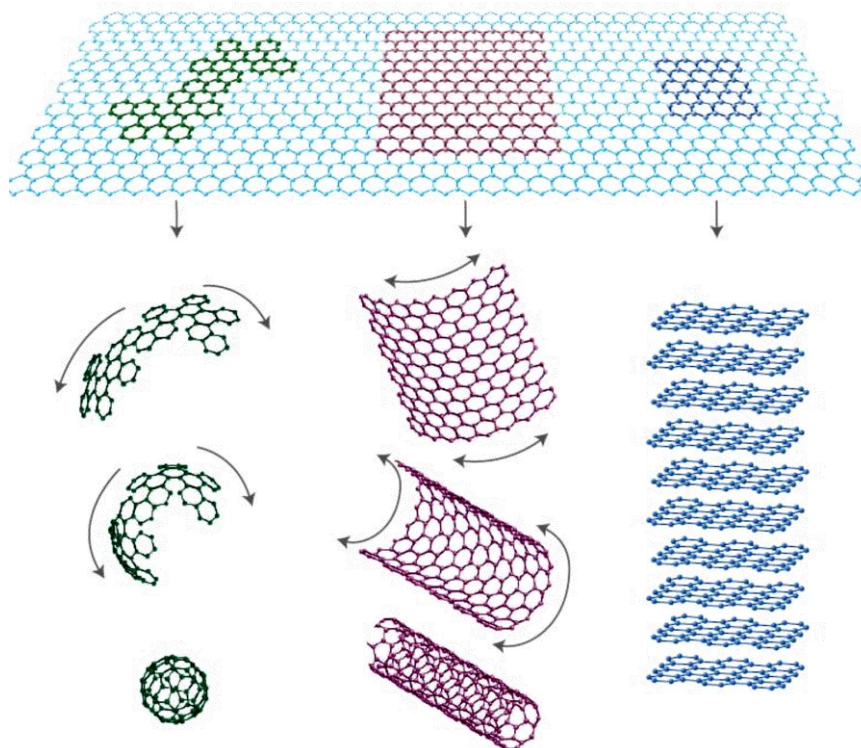
Figure 2.13. C_{60} fullerene molecules, carbon nanotubes, and graphite can all be thought of as being formed from graphene sheets [98].

The concept of graphene has been around for more than 170 years and there have been many studies to obtain graphene chemically [99,100]. The earliest reports for this field can be traced back to the 1840s, when the intercalation which can be described as the insertion of a small-molecule species, such as an acid or alkali metal, in between the carbon layers and exfoliation of graphite with sulfuric and nitric acids was discussed by Schafhaeutl [100,101]. In 1859, B. C. Brodie made some modifications to characterize the molecular weight of graphite, where the graphite was treated with a mixture of

$KClO_3$ and nitric acid [102,103]. P.R. Wallace conducted theoretical studies on the electronic structure of graphene and noted the linear dispersion relation in 1947 [104]. In 1958, graphene was synthesized by Hummers and Offeman by using a mixture of sulfuric acid, sodium nitrate, and potassium permanganate to oxidize graphite [105]. In 1956, the wave equation for excitations of graphene was studied by J.W. McClure [106], and in 1984, G.W. Semenoff discussed the similarity to the Dirac equation [107]. In 1997, IUPAC formalized the definition of graphene: "The term graphene should be used only when the reactions, structural relations or other properties of individual layers are discussed." [108] Although it was stated by Landau and Peierls more than 70 years ago this material was thermodynamically unstable and could not exist [109,110], first evidence of single layer graphene was explored by Geim and Novoselov in 2004 [111] who later on won the Nobel Prize in Physics 2010 for their studies on graphene [21].

2.4.1. Synthesis of Graphene

Graphene can either be prepared in a bottom up fashion by assembling smaller molecules together or by a top down approach, such as exfoliation of graphene [112]. Graphene synthesis methods include exfoliation and cleavage [111,113], Chemical Vapor Deposition (CVD) techniques [114,115] and other processing routes [116,117,118,119].

2.4.2. Properties of Graphene

Graphene, being only one atom thick (i.e. having an height of 0.33 nm), is the thinnest material ever known [98]. It is a transparent conductor [120] and mechanically lighter, stronger, harder and more flexible than steel. In addition, graphene and its bilayer form behave as zero-gap semiconductors or in other words as zero-overlap semimetals [111].

Free-standing monolayer graphene has second-order elastic stiffness of 340 Nm^{-1} and breaking strength of 42 Nm^{-1} which indicates that the graphene is one of the strongest materials ever observed [121].

Graphene's thermal conductivity is ten times better than copper (ca. 5000 Wm^{-1}K^{-1}) [122]; and it has unique electronic properties including an unusual quantum Hall effect which describes the electron transport in graphene by a Dirac-like equation [111]. Its electrical conductivity (ca. 10^6 Ω^{-1}cm^{-1} at room temperature) is much higher than that of silver; and it has extraordinary breakdown current density exceeding 10^8 A/cm^2 [123]; and very high charge carrier mobilities (up to 200000 cm^2/Vs at room temperature, more than hundred times larger than bulk silicon) [98,124,125].

Moreover, with a negative thermal coefficient [126,127] graphene can extend elastically up to 20% while cooling and shrink while heating unlike any other crystal without breaking [128]. It is also thermally stable up to 2300 K (ca. 500 °C in air) [129].

CHAPTER 3

EXPERIMENTAL

3.1. Materials

Ammonia borane (NH$_3$BH$_3$, AB, Aldrich, 97%), ruthenium(III) chloride trihydrate (RuCl$_3$.3H$_2$O, Sigma Aldrich, 99.9%), potassium permanganate (KMnO$_4$, Merck, 99.5%), hydrogen peroxide (H$_2$O$_2$, Merck 30%), sodium nitrate (NaNO$_3$, Aldrich, 99%), sulfuric acid (H$_2$SO$_4$, Merck, 96%), graphite powder (99.85%) were purchased and used as received. Distilled water was used as the reaction solvent. All glassware and Teflon coated stirrer bars were washed with acetone, followed by copious rinsing with distilled water before drying in oven at 150 °C.

3.2. Experimental Procedure

3.2.1. Preparation of Graphene Oxide

Graphene oxide was prepared by Hummers method [105] modified by Zhou et al [130] from graphite powder following a previously described procedure. Briefly i) 2.0 g of graphite powder and 1.5 g of NaNO$_3$ were added into 150 mL of 98% H$_2$SO$_4$ solution in a round-bottom flask (500 mL) immersed in an ice bath. ii) While stirring, 9.0 g of KMnO$_4$ was added slowly and allowed to dissolve. iii) The mixture was stirred for 3 days at room temperature. iv) 20 mL of 30% H$_2$O$_2$ was added into the solution and the

solution was stirred for one more hour in order to completely react with the remaining $KMnO_4$ after three days. The resulting precipitate was collected on a funnel with sintered glass filter (medium frit) and washed by 3% H_2SO_4 (500 mL), 10% HCl (500 mL) and then H_2O until the pH value of the filtrate solution reached at 7.00. 500 mg of graphene oxide was obtained after drying the remnant in an oven at 120 ºC for 12 h.

3.2.2. Preparation of Ruthenium(0) Nanoparticles Supported on Graphene

The dried graphene powder (500 mg) was stirred in 100 mL of an aqueous solution of 42.1 mg of $RuCl_3.3H_2O$ (0.16 mmol = 1.6 mM) for 72 h at room temperature. In order to obtain a uniform dispersion ultrasonification was applied. Ammonia borane (90 mg = 2.92 mmol) was added to the suspension under stirring. Hydrogen evolution started immediately and the color of the solution turned to black. When the hydrogen evolution was completed ruthenium(0) nanoparticles supported on graphene was left to precipitate. The supernatant solution was removed and the solid was washed with 100 mL of distilled water and the remnant was dried in an oven at 120 ºC for 12 h.

3.3. Characterization of Ruthenium(0) Nanoparticles Supported on Graphene

3.3.1. Powder XRD (X-Ray Diffraction)

X-Ray Diffraction (XRD) pattern was recorded on a Rigaku Miniflex diffractometer with CuKα (30 kV, 15 mA, λ= 1.54051 Å), over a 2θ range from 5 to 90° at room temperature.

3.3.2. Scanning Electron Microscope (SEM) and Electron Diffraction X-Ray (EDX)

Scanning electron microscope (SEM) and electron diffraction X-ray (EDX) data were acquired using a Zeiss EVO40 environmental SEM that is equipped with a LaB6 electron gun, a vacuum SE detector, an elevated pressure SE detector, a backscattering electron detector (BSD), and a Bruker AXS XFlash 4010 detector. Samples for SEM and EDX analysis were prepared by grinding the powder samples into fine particles and mechanically dispersing them on an electrically conductive carbon film which was placed on an aluminum sample holder. No additional coatings or dispersive liquids were used for the SEM and EDX sample preparation. SEM images were obtained using a vacuum SE detector where electron acceleration voltage of the incident beam was varied within 10-20 kV and the samples were kept typically at $\leq 5 \times 10\text{-}5$ Torr inside the SEM. All of the EDX data were collected using an electron acceleration voltage of 20 kV and a working distance of 15 mm.

3.3.3. Transmission Electron Microscope (TEM)

Transmission electron microscope (TEM) images were obtained using a JEM-2100 (JEOL) instrument operating at 200 kV. The nanoparticles solution prepared as described in the section 4.2 was centrifuged at 6000 rpm for 10 min. Then, the nanoparticles sample was redispersed in 5 mL distilled water. One drop of the diluted colloidal solution was deposited on the silicon oxide coated copper grid and evaporated under inert atmosphere. Samples were examined at magnifications between 100 and 800k. Particle size of the nanoparticles is calculated by using NIH image software from the TEM image by counting non-touching particles. Size distributions are quoted as the mean diameter ± the standard deviation.

3.3.4. Inductively Coupled Plasma Optical Emission Spectroscopy (ICP-OES)

The ruthenium contents of the ruthenium(0) nanoparticles supported on graphene samples after centrifugation were determined by ICP-OES (Inductively Coupled Plasma Optical Emission Spectroscopy, Leeman-Direct Reading Echelle) after each sample was completely dissolved in the mixture of HNO_3/HCl (1/3 ratio). For ICP-OES analysis, a calibration curve was prepared by measuring the absorption of 0, 1, 2, 5, 10 and 20 ppm of standard solution of Ru. Then, the absorption of the samples of ruthenium(0) nanoparticles supported on graphene was measured and the Ru content of the samples was determined from the calibration curve.

3.4. Testing the Catalytic Activity of Ruthenium(0) Nanoparticles Supported on Graphene in the Hydrolysis of Ammonia Borane

The catalytic activity of ruthenium(0) nanoparticles supported on graphene were tested in hydrogen generation from the hydrolysis of ammonia borane, by measuring the rate of hydrogen generation. To determine the rate of hydrogen generation, a jacketed reaction flask (50 mL) containing a Teflon-coated stir bar was placed on a magnetic stirrer (WiseStir MSH-20A) and thermostated to 25.0 ± 0.1 °C by circulating water through its jacket from constant temperature bath. In order to be able to observe the hydrogen gas evolved from the reaction, a graduated glass tube filled with water was connected to the jacketed flask. After that, portions of ruthenium(0) nanoparticles supported on graphene in 10 mL water were transferred into the jacketed reaction flask and stirred until it reached the thermal equilibrium. Then 1.0 mmol (31.8 mg) of ammonia borane, NH_3BH_3, (corresponding to maximum amount of hydrogen, H_2, gas of 3.0 mmol (80.7 mL at 25.0 ± 0.1 °C temperature and 0.908 atm pressure) was added to the solution containing the catalyst. The jacketed reaction flask was sealed by a septum

to prevent the loss of gaseous components and stirred at 800 rpm while the reaction was followed until there was no release of H_2 gas.
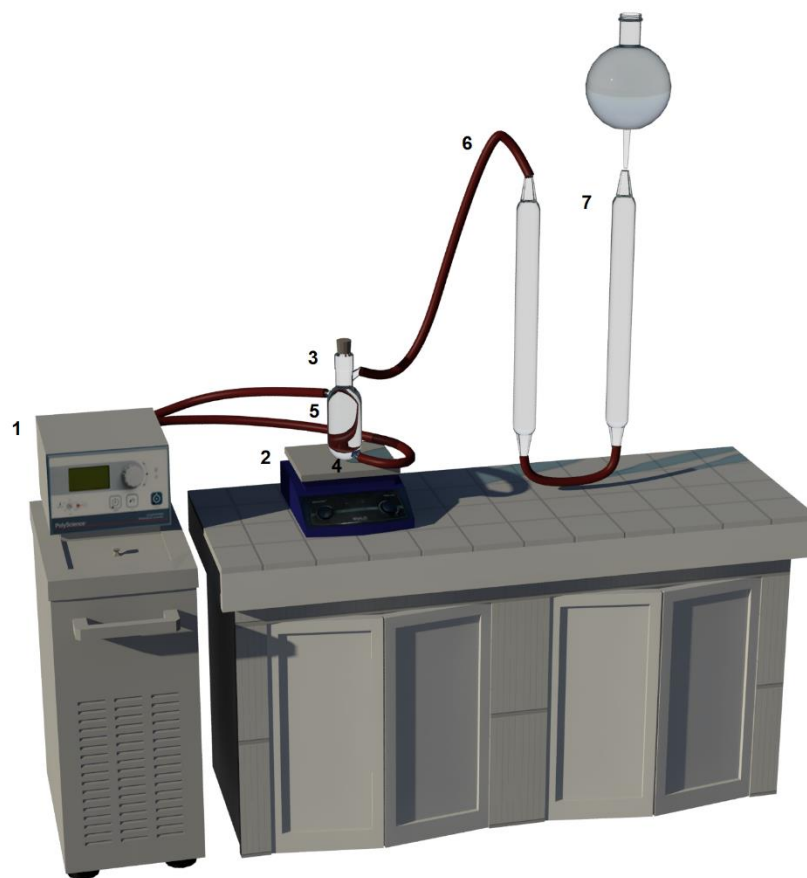
Figure 3.1. The experimental setup used in performing the catalytic hydrolysis of ammonia borane and measuring the hydrogen generation rate. **1**: Water Bath Circulator, **2**: Magnetic Stirrer, **3**: Jacketed Schlenk Tube, **4**: Water in, **5**: Water out, **6**: Plastic Hose, **7**: Burette Filled with Water.

3.5. Kinetics of the Hydrolysis of Ammonia Borane Catalyzed by Ruthenium(0) Nanoparticles Supported on Graphene

In order to establish the rate law for catalytic hydrolysis of NH_3BH_3 using ruthenium(0) nanoparticles supported on graphene, three different sets of experiments were performed in the same way as described in the section "testing the catalytic activity of ruthenium(0) nanoparticles supported on graphene in the hydrolysis of ammonia borane". In the first set of experiments, the hydrolysis reaction was performed starting with different initial concentration of ruthenium(0) (0.057, 0.115, 0.172, 0.230, 0.287 mM) were performed at room temperature (25.0 ± 0.1 °C) while the initial ammonia borane concentration was kept constant at 100 mM (31.8 mg = 1.00 mmol). The second set of experiments were performed at room temperature (25.0 ± 0.1 °C) by keeping the initial concentration of ruthenium(0) constant at 0.287 mM and varying the NH_3BH_3 concentration (50, 100, 150, 200, 250 mM). Finally, the hydrolysis of ammonia borane was performed in the presence of ruthenium(0) nanoparticles at constant catalyst (0.12 mM) and substrate (100 mM) concentrations and various temperatures in between 20 and 40 °C in order to obtain the activation energy (E_a), enthalpy ($\Delta H^{\ddagger}$), and entropy ($\Delta S^{\ddagger}$) of activation.

3.6. Determination of the Catalytic Lifetime of Ruthenium(0) Nanoparticles Supported on Graphene in the Hydrolysis of Ammonia Borane

Catalytic lifetime of ruthenium(0) nanoparticles supported on graphene in the hydrolysis of ammonia borane was determined by measuring the total turnover number, TTON, of the reaction. The experiment was conducted by starting with 50 mL aqueous solution of graphene supported ruthenium(0) nanoparticles catalyst containing 15 mg Ru (0.0017 mmol) and adding 200 mg AB (6.29 mmol) at 25.0 ± 0.1 °C where the evolution of H_2

gas was monitored. When the stoichiometric H_2 gas (3.0 mol H_2/mol AB) generation was achieved, a new batch of ammonia borane was added into the solution. The procedure was repeated until H_2 gas was no longer released.

3.7. Reusability of Ruthenium(0) Nanoparticles Supported on Graphene Catalyst in the Hydrolysis of Ammonia Borane

Reusability of ruthenium(0) nanoparticles supported on graphene catalyst in the hydrolysis of ammonia borane was tested by measuring the rate of hydrogen generation in successive runs of the experiment. The experiment was started with 10 mL aqueous solution of graphene supported ruthenium(0) nanoparticles catalyst containing 40 mg Ru (0.0046 mmol = 0.46 mM) and 31.8 mg AB (1.00 mmol = 100 mM) at 25.0 ± 0.1 °C. After the release of stoichiometric H_2 gas (3.0 mol H_2/mol AB), the catalyst was isolated from the reaction solution by centrifugation and washed with 3×30 mL water. The isolated catalyst was redispersed in 10 mL water and 31.8 mg AB (1.00 mmol = 100 mM) was added. The hydrolysis was started and the hydrogen release was monitored at 25.0 ± 0.1 °C. This procedure was repeated throughout 9 more experiments and results were expressed as the percentage of initial catalytic activity of Ru(0)/Graphene in the successive hydrolysis of ammonia borane.

CHAPTER 4

RESULTS AND DISCUSSION

4.1. Preparation and Characterization of Graphene Oxide

The first step of this study was the preparation of graphene oxide. Graphene oxide was prepared from graphite powder by Hummers method [105] modified by Zhou et al [130]. After the addition of graphite powder and $NaNO_3$ into H_2SO_4 solution in an ice bath, $KMnO_4$ was added slowly to prevent the sudden accumulation of heat evolved. After 3 days stirring at room temperature H_2O_2 was added into the solution to remove the unreacted $KMnO_4$. The solid materials was then isolated by filtration and washed with H_2SO_4, HCl and H_2O until the filtrate reached neutral pH. Graphene oxide was obtained after drying the precipitate.

Graphene oxide was characterized by using SEM which gives information about the surface of the material. As illustrated in Figure 4.1. (a) graphite has a rock like structure, while in (b) graphene oxide has a silky texture which indicates that the graphite is reduced to a few layers.
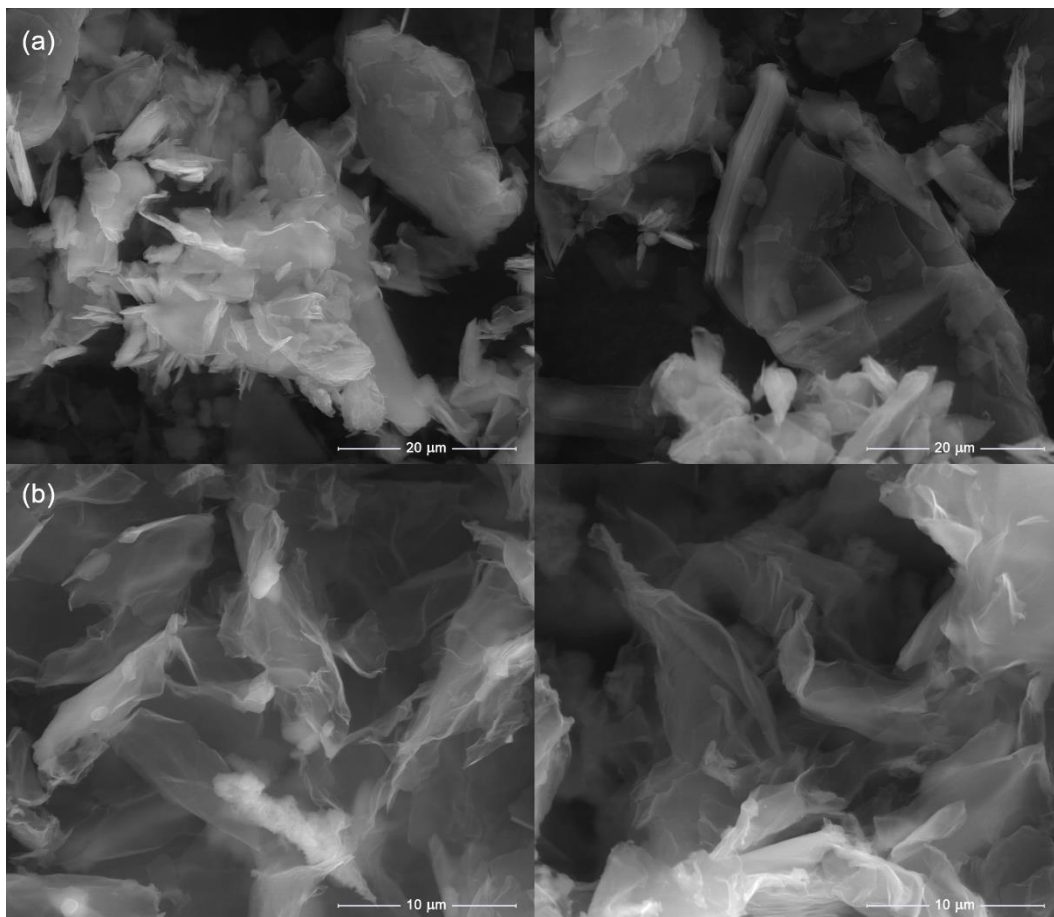
Figure 4.1. SEM images of (a) commercially available graphite (purchased from Sigma Aldrich) with a scale bar of 20 μm and (b) synthesized graphene oxide with a scale bar of 10 μm.

4.2. Preparation and Characterization of Ruthenium(0) Nanoparticles Supported on Graphene

After the preparation of the graphene oxide by modified Hummers' method, the dried graphene oxide powder (500 mg) was dispersed in 100 mL of an aqueous solution of 42.1 mg of $RuCl_3.3H_2O$ (0.16 mmol = 1.6 mM) by ultrasonification. Then, the suspention was stirred for 72 h at room temperature. The reduction of ruthenium(III) ions to ruthenium(0) nanoparticles supported on graphene was achieved by using ammonia borane as reducing agent. Cheng et al used methylamine borane, $CH_3NH_2BH_3$ for the same reduction [22]. Then ruthenium(0) nanoparticles supported on graphene was isolated from the reaction medium by filtration on a medium glass frit and characterized by using a combination of advanced analytical methods including ICP-OES, XRD, SEM, SEM/EDX, and TEM. Figure 4.2 shows powder XRD patterns of graphene oxide and ruthenium(0) nanoparticles supported on graphene. On passing from graphene oxide to the ruthenium(0) nanoparticles supported on graphene, the intense peak of graphene oxide disappears while new peaks at around 25.2° and 42.5° appear which are attributed to graphene indicating that the graphene oxide is successfully reduced to graphene [131]. Although no Bragg peak is observable for ruthenium due to the low loading (1.16 % wt), one has to keep in mind that a weak ruthenium peak might be hidden under the broad band of graphene [131].
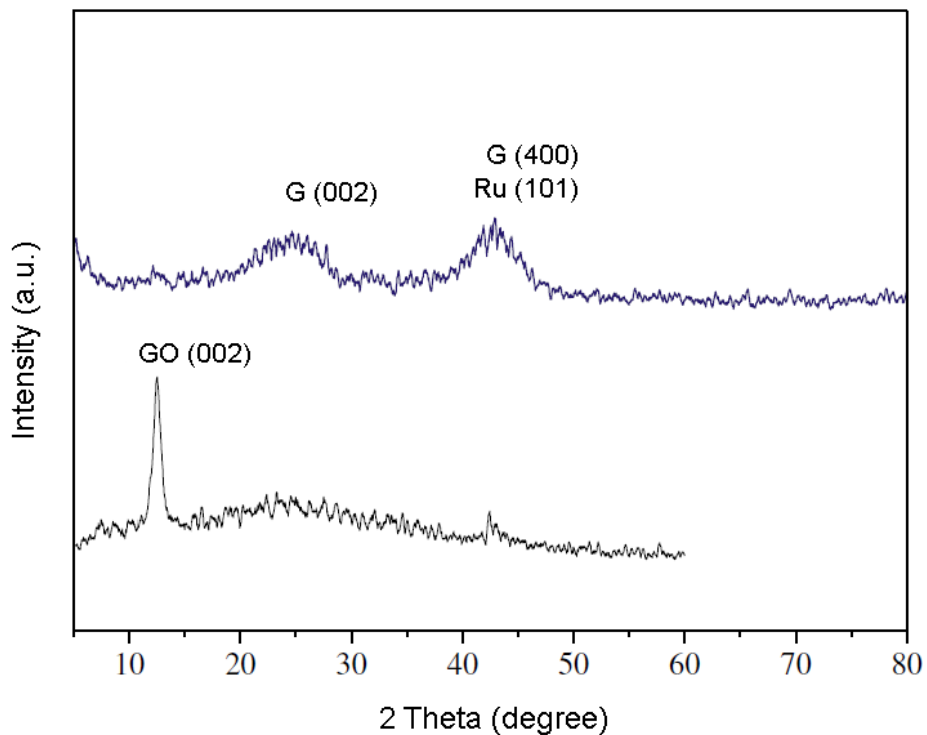
Figure 4.2. Powder X-Ray Diffraction (P-XRD) patterns of graphene oxide and ruthenium(0) nanoparticles supported on graphene.

The ruthenium content of the materials prepared, Ru(0)/graphene, was determined by the inductively coupled plasma – optical emission spectroscopy, ICP-OES, and was found to be 1.16 % wt.

The next technique used to characterize the prepared Ru(0)/graphene was SEM (Figure 4.3. (a), (b)), which exhibits that no bulk ruthenium metal was formed. However, the

SEM/EDX analysis (Figure 4.3. (c)) clearly indicates the presence of ruthenium, likely in the form of nanoparticles supported on the graphene [132].

The SEM/EDX spectrum exhibits K_α line at 3.30 KeV and K_β line at 3.60 KeV for potassium and K_α line at around 5.90 KeV for manganese, which can be attributed to the $KMnO_4$ still present in the sample.

There is also K_α line at 2.30 KeV for sulfur which might indicate that H_2SO_4 could not be removed from the sample in the washing process. The residues of both $KMnO_4$ and H_2SO_4 may cause a negative effect on the activity of the catalyst by attaching on the surface of graphene and preventing the ruthenium atoms to support on it.
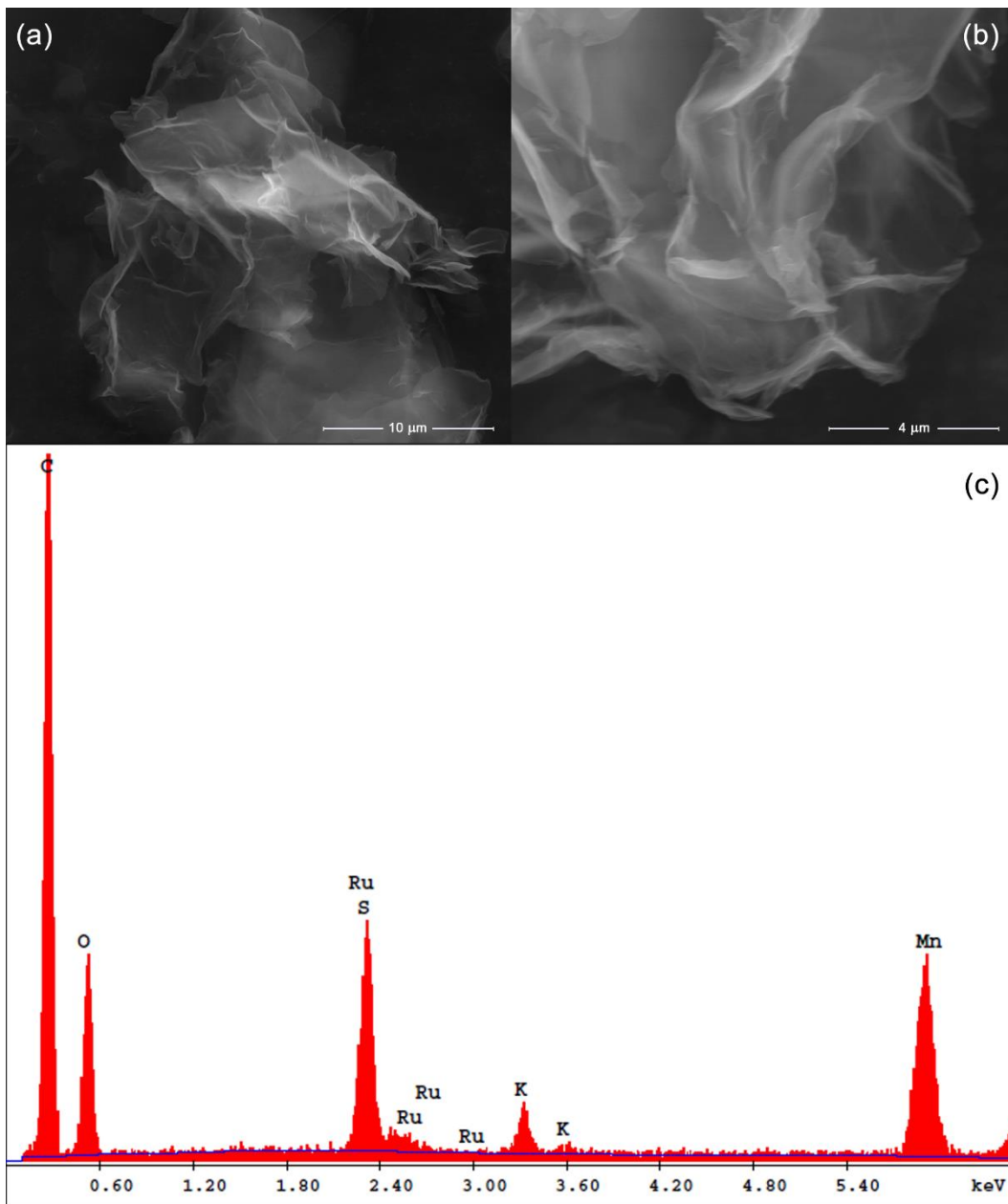
Figure 4.3. SEM images of Ru(0)/Graphene (a) with a scale bar of 10 μm, (b) with a scale bar of 4 μm and (c) SEM-EDX spectrum of Ru(0)/Graphene with a 1.16 % wt Ru loading.

One of the most efficient methods in characterization of the metal nanoparticles is the Transmission Electron Microscopy (TEM) which gives information about size, shape and size distribution of nanoparticles. Figure 4.4 shows the TEM images of ruthenium nanoparticles supported on graphene. It can be seen from the images and histogram that the well dispersed ruthenium(0) nanoparticles were formed on the surface of graphene support. NIH image was used to get the mapping [133] and count the number of particles on the catalyst from the TEM image and the mean particle size of ruthenium(0) nanoparticles was found to be as 1.9 ± 0.8 nm while the recent paper has reported a particle size of 1.7 nm for the ruthenium(0) nanoparticles supported on graphene [22]. The observation of a tail at right side of histogram indicates that the formation of ruthenium(0) nanoparticles has not been completed yet. The ruthenium(0) nanoparticles must have been harvested when they were still growing.
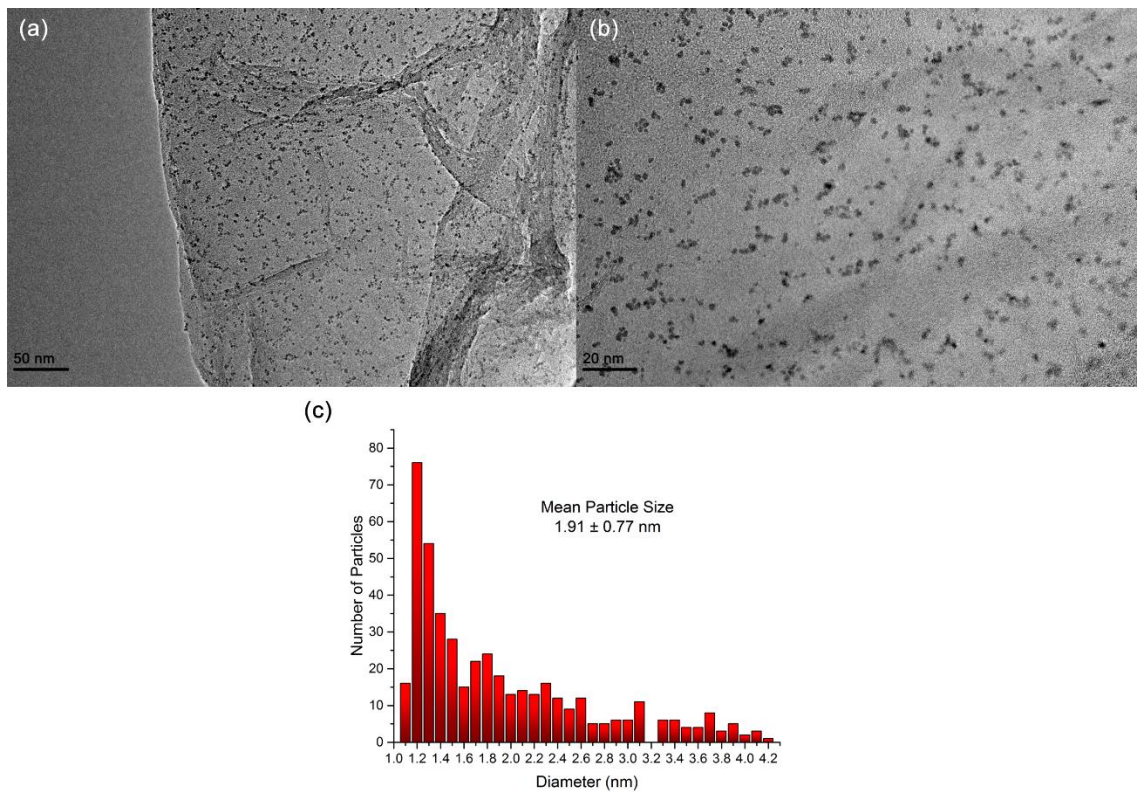
Figure 4.4. TEM images of Ru(0)/Graphene with a scale bar of (a) 50 nm, (b) 20 nm and (c) corresponding particle size histogram.

4.3. Kinetics of the Hydrolysis of Ammonia Borane Catalyzed by Ruthenium(0) Nanoparticles Supported on Graphene

After the preparation and characterization of the well dispersed ruthenium(0) nanoparticles supported on graphene, they were tested as catalyst in hydrogen generation from the hydrolysis of ammonia borane. The ruthenium(0) nanoparticles supported on graphene were found to be highly active catalyst in hydrogen generation from the hydrolysis of ammonia borane at low concentrations and room temperature releasing 3.0 equivalent H_2 gas per mole of NH_3BH_3 as shown in Figure 4.5. The plot of equivalent H_2 per mole of ammonia borane in Figure 4.5 shows the release of 3.0 equivalent hydrogen in the hydrolysis of 100 mM NH_3BH_3 started with Ru(0)/Graphene as catalyst in 0.287 mM ruthenium concentration at 25.0 ± 0.1 °C. The curve exhibits a sigmoidal shape $\left(\sim \frac{1}{1+e^{-kx}} \right)$ where the k value is directly proportional to the ruthenium concentration. A short induction period, during which the precursor ruthenium species are converted into their active forms, is followed by a rapid hydrogen generation. Then, the hydrogen release continues almost linearly until the complete consumption of all ammonia borane.
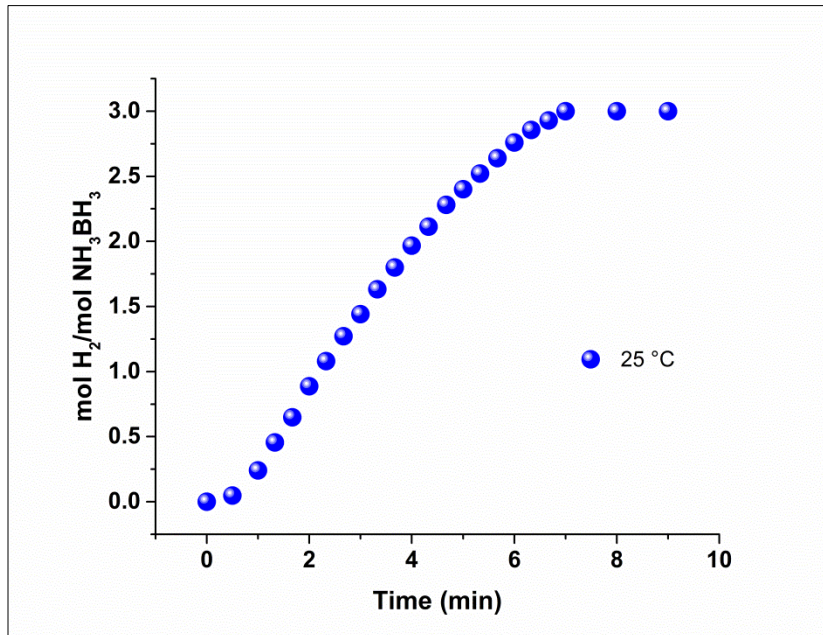
Figure 4.5. Plot of mol H_2/mol NH_3BH_3 versus time for the hydrolysis of ammonia borane. Ru concentration [Ru] = 0.287 mM, the substrate concentration [NH_3BH_3] = 100 mM at 25 ± 0.1 °C.

Figure 4.6 shows the evolution of equivalent hydrogen per mole of ammonia borane during the hydrolysis of 100 mM NH_3BH_3 started with Ru(0)/Graphene as catalyst in different ruthenium concentration at 25.0 ± 0.1 °C. All the plots exhibit sigmoidal shape with a short induction period. The unreactive species are converted to their active forms during the induction period. Then, a rapid hydrogen generation starts and continues almost linearly until the consumption of all ammonia borane present in the solution. The hydrogen generation rate was found to be directly proportional to the ruthenium

concentration. For all tests a complete hydrogen release (mol H_2/mol H_3NBH_3 = 3) was observed.
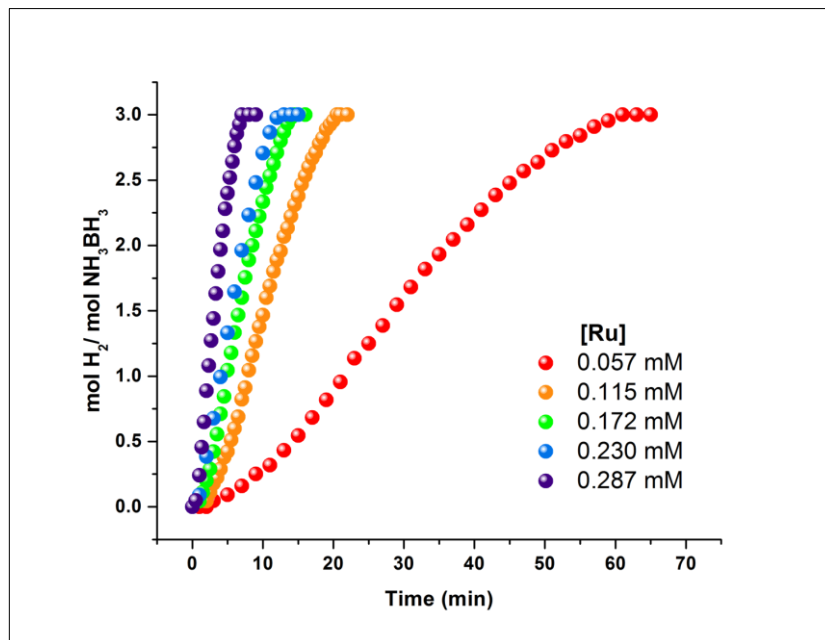
Figure 4.6. Plot of mol H_2/mol NH_3BH_3 versus time for the hydrolysis of ammonia borane starting with Ru(0)/Graphene (with a ruthenium content of 1.16 wt.%) in different Ru concentrations [Ru] = 0.057, 0.115, 0.172, 0.230, 0.287 mM, the substrate concentration [NH_3BH_3] = 100 mM at 25.0 ± 0.1 °C.

The hydrogen generation rate was determined from the slope measured in the nearly linear portion of the plot for each concentration of ruthenium(0) nanoparticles. Figure 4.7 shows the plot of hydrogen generation rate *versus* initial concentration of ruthenium, both in logarithmic scale, which gives a straight line with a slope of 1.08 indicating that hydrolysis of ammonia borane is first order with respect to the ruthenium concentration.
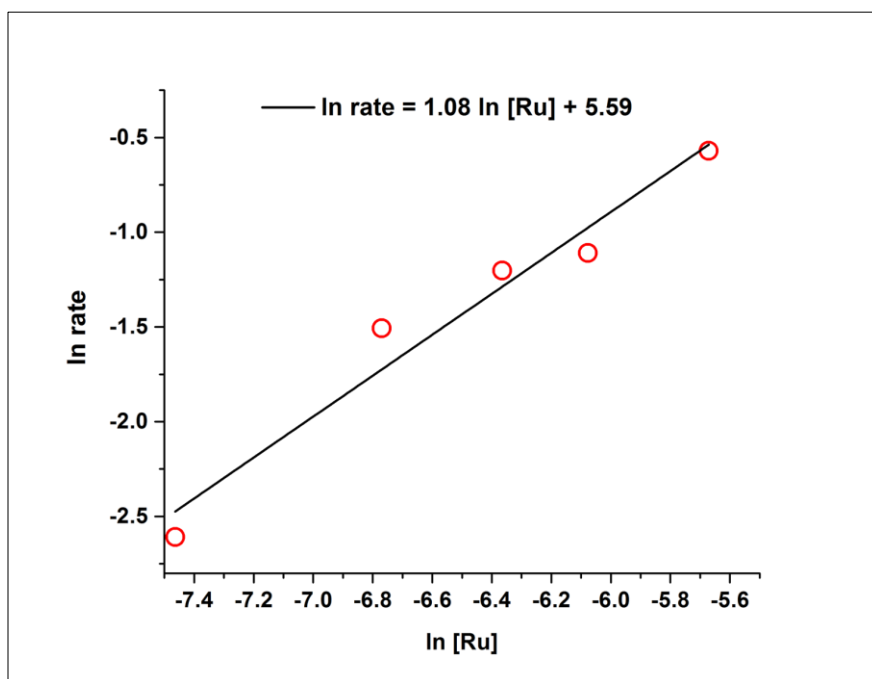
Figure 4.7. Plot of hydrogen generation rate versus the concentration of ruthenium in logarithmic scale for the hydrolysis of ammonia borane in different Ru concentrations [Ru] = 0.057, 0.115, 0.172, 0.230, 0.287 mM, the substrate concentration $[NH_3BH_3]$ = 100 mM at 25.0 ± 0.1 °C.

The effect of NH_3BH_3 substrate concentration on the hydrogenation rate was also studied by performing a series of experiments starting with different initial concentration of NH_3BH_3 while keeping the ruthenium concentration constant at 0.287 mM. Figure 4.8 illustrates the hydrogen generation plots for the hydrolysis of ammonia borane in various initial ammonia borane concentrations. It can be seen that slopes of the rate curves do not linearly accommodate to ammonia borane concentration in the reaction medium which has negligible effect on the rate of hydrogen generation.

The rate of hydrogen generation from catalytic hydrolysis of ammonia borane is independent of AB concentration as evidenced by almost matching slopes of near-linear sigmoidal curves. The hydrogen generation rate was determined from the linear portion of each plot. For all tests a complete hydrogen release (mol H_2/mol H_3NBH_3 = 3) was observed.
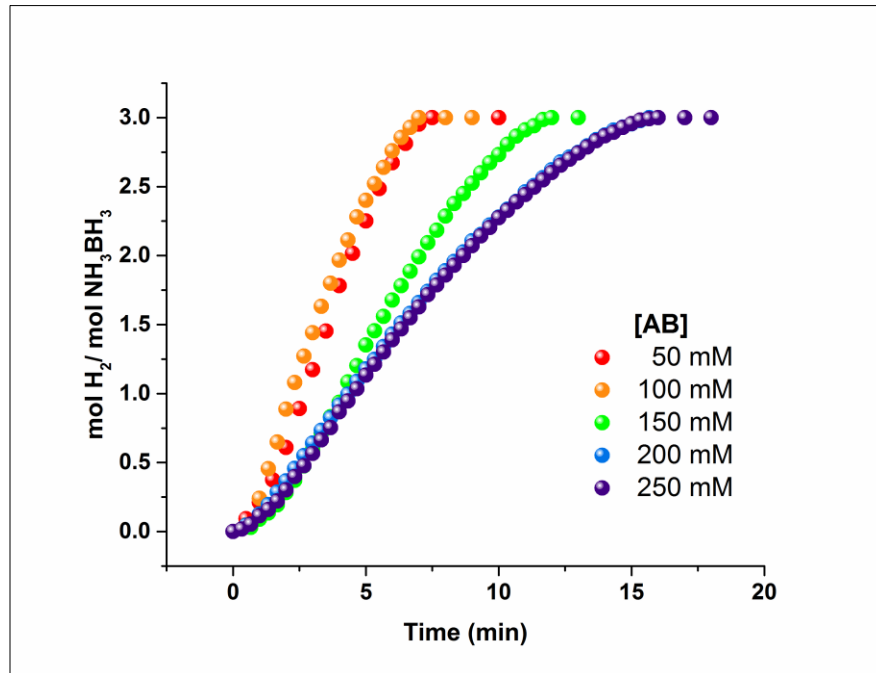
Figure 4.8. Plot of mol H_2/mol NH_3BH_3 versus time for the hydrolysis of ammonia borane in various ammonia borane concentrations $[NH_3BH_3]$ = 50, 100, 150, 200, 250 mM, the catalyst concentration $[Ru]$ = 0.287 mM at 25.0 ± 0.1 °C.

The slope of the line fitted to the experimental data shown in Figure 4.9 is very small indicating that the hydrolysis reaction can be assumed to be zero order with respect to the concentration of NH_3BH_3.
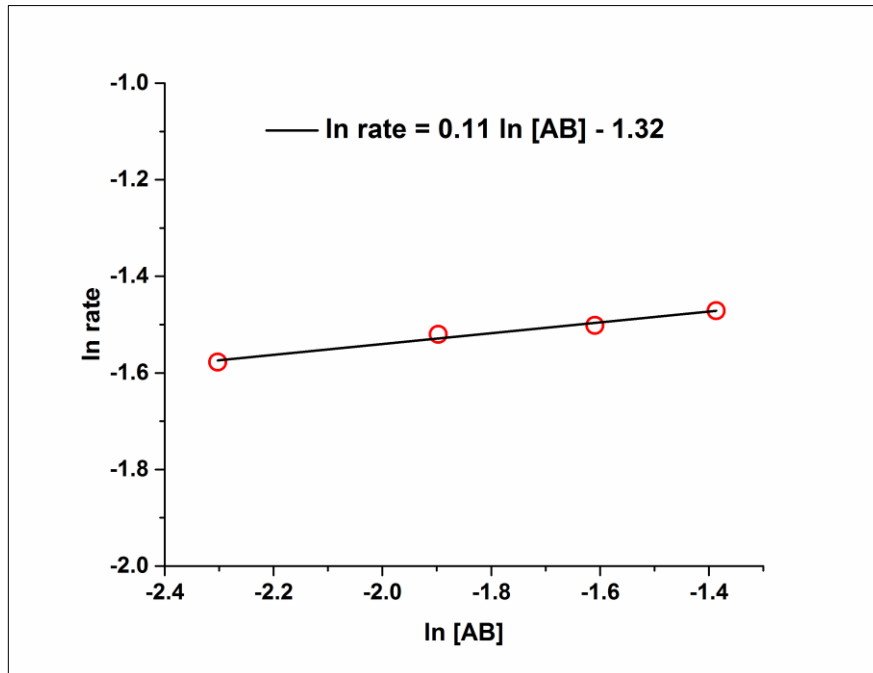
Figure 4.9. Plot of hydrogen generation rate versus the concentration of ammonia borane in logarithmic scale for the hydrolysis of ammonia borane in various ammonia borane concentrations $[NH_3BH_3]$ = 50, 100, 150, 200, 250 mM, the catalyst concentration $[Ru]$ = 0.287 mM at 25.0 ± 0.1 °C.

Thus, the rate law for the catalytic hydrolysis of ammonia borane can be given as;

$$-3\frac{d[NH_3BH_3]}{dt} = \frac{d[H_2]}{dt} = k[Ru] \qquad (4.1)$$

Both ruthenium(0) nanoparticles catalyzed and hydrolysis of ammonia borane were carried out at various temperature in the range of 20-40 °C starting with the initial

59

substrate concentration of 100 mM NH_3BH_3 and an initial catalyst concentration of 0.115 mM ruthenium.
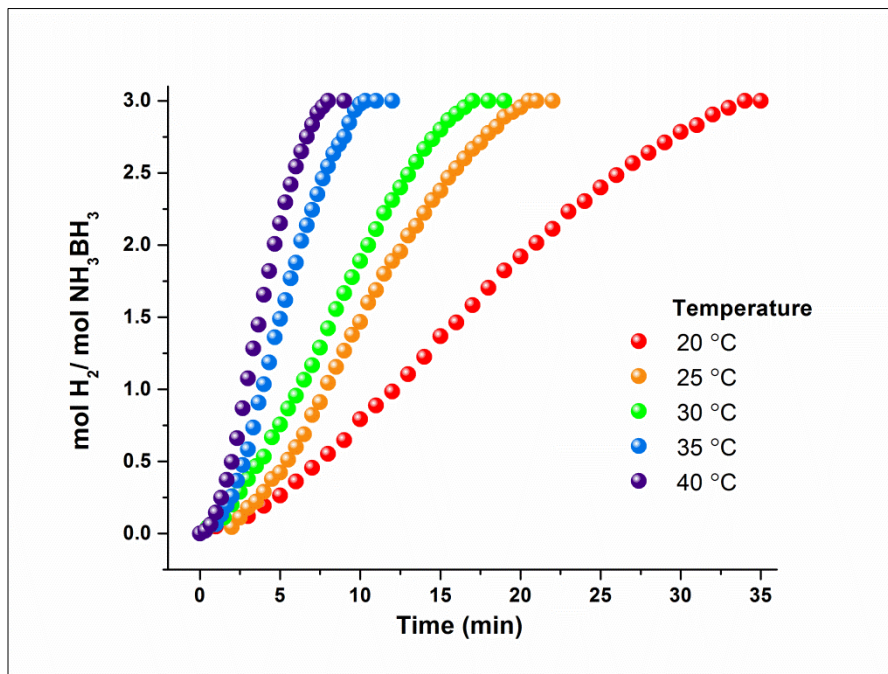
Figure 4.10. Plot of mol H_2/mol NH_3BH_3 versus time for the hydrolysis of ammonia borane in various temperatures, T = 20, 25, 30, 35, 40 °C, the catalyst concentration [Ru] = 0.115 mM, the substrate concentration [NH_3BH_3] = 100 mM.

The rate of hydrogen generation from hydrolysis of ammonia borane by using ruthenium(0) nanoparticles supported on graphene increases with increasing temperature. The induction period is inversely proportional to the temperature since slopes of the curves are observed to increase more rapidly at higher temperatures. For all tests a complete hydrogen release (mol H_2/mol H_3NBH_3 = 3) was observed.

The values of rate constant were calculated from the slopes of the rate of ruthenium(0) nanoparticles catalyzed hydrolysis of ammonia borane. They are listed in Table 4.1.

Table 4.1. Rate constants for the hydrolysis of ammonia borane catalyzed by Ru(0) nanoparticles.

Temperature (°C)	Rate Constant, k ([NH$_3$BH$_3$].[mol Ru(0)]$^{-1}$.s^{-1})
20	0.115
25	0.230
30	0.236
35	0.441
40	0.544

The rate constant/temperature data was evaluated according to the Arrhenius equation and Eyring equation to obtain the energy, enthalpy and entropy of activation. First, the Arrhenius equation was used for the evaluation:

$$k = Ae^{-\frac{E_a}{RT}} \qquad\qquad (4.2)$$

where A and E_a are constants characteristics of the reaction and R is the gas constant. E_a is the Arrhenius activation energy and A is the pre-exponential factor [87]. Taking the natural logarithm of Equation 4.2, gives Equation 4.3:

$$\ln k = \ln A - \frac{E_a}{RT} \qquad\qquad (4.3)$$

Figure 4.11 shows the Arrhenius plot, ln k versus the reciprocal absolute temperature (1/T). Slope of the straight line gives an activation energy of 57 ± 1 kJ mol^{-1} for hydrogen generation from the hydrolysis of ammonia borane catalyzed by ruthenium(0) nanoparticles supported on graphene.

Since k is proportional to the exponential of T^{-1}, random fluctuations in temperature cause higher deviations in the rate at low temperatures therefore increasing the temperature decreases the standard deviation as observed in Figure 4.11.

Figure 4.11. The Arrhenius plot, lnk versus the reciprocal absolute temperature 1/T, for the hydrolysis of ammonia borane catalyzed by ruthenium(0) nanoparticles supported on graphene in the temperature range is 20 - 40 °C.

The activation energy for the hydrolytic dehydrogenation of ammonia borane catalyzed by Ru(0)/Graphene is comparable to the literature values reported for the same reaction using other ruthenium catalysts: 28 kJ mol^{-1} for ruthenium nanoparticles stabilized by ZK-4 zeolite framework (RuNPs@ZK-4) [134], 33 kJ mol^{-1} for ruthenium(0) nanoparticles supported on multiwalled carbon nanotubes (Ru(0)@MWCNTs) [135], 34.8 kJ mol^{-1} for ruthenium nanocluster catalyst supported on carbon black (Ru/C) [136], 47 kJ mol^{-1} for laurate stabilized Ru(0) nanoclusters [137], 48 kJ mol^{-1} for ruthenium nanoparticles supported on aluminum oxide nanopowder (Ru@Al$_2$O$_3$) [138],

54 kJ mol^{-1} for water-soluble poly(4-styrenesulfonic acid-co-maleic acid) stabilized ruthenium(0) nanoclusters (Ru(0)NP/PSSA-co-MA) [139], 58 kJ mol^{-1} for hydroxyapatite supported ruthenium(0) nanoparticles catalyst (Ru(0)@HAp) [140], 76 kJ mol^{-1} for ruthenium supported on carbon (Ru/carbon) [141], 77 kJ mol^{-1} for ruthenium(0) nanoparticles supported on xonotlite nanowire (Ru(0)@X-NW) [142] (Figure 4.12). In a similar study conducted by using the Ru(0)/Graphene catalyst the apparent activation energy was determined to be approximately 11.7 kJ mol^{-1}, which is the lowest value ever reported in the catalytic hydrolytic dehydrogenation of ammonia borane [22]. This discrepancy can be attributed to the differences in the pathways for synthesis of the catalyst hence its morphological nature.
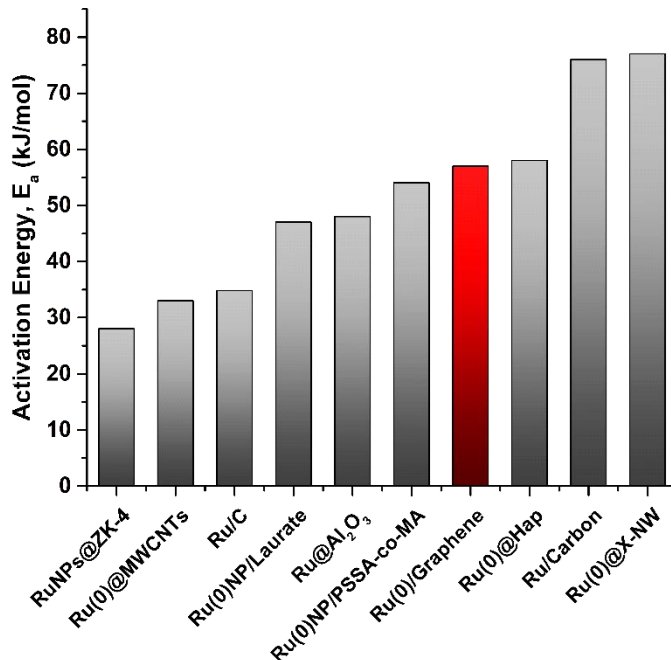
Figure 4.12. Activation energy of reported ruthenium catalysts (Ea = kJ/mol) in hydrolytic dehydrogenation of ammonia borane [134-142].

The enthalpy of activation, $\Delta H^{\ddagger}$ and the entropy of activation, $\Delta S^{\ddagger}$ were calculated from the Eyring equation, Equation 4.4, by plotting the graph of ln k/T versus 1/T,

$$\ln\frac{k}{T} = \frac{1}{T}\left(-\frac{\Delta H^{\ddagger}}{R}\right) + \ln\frac{k_b}{h} + \frac{\Delta S^{\ddagger}}{R} \qquad (4.4)$$

Figure 4.13 shows the Erying plot, ln (k/T) versus reciprocal absolute temperature (1/T). The slope of the straight line gives an enthalpy of activation of 55 ± 1 kJ mol^{-1} and the intercept gives entropy of activation of -75 ± 3 J (mol.K)$^{-1}$. The small value of activation

enthalpy and the large negative value of activation entropy are indicative of an associative mechanism for the ruthenium(0) nanoparticle catalyzed hydrolysis of ammonia borane, consistent with the mechanism suggested for the hydrolysis of ammonia borane given in the literature [143].
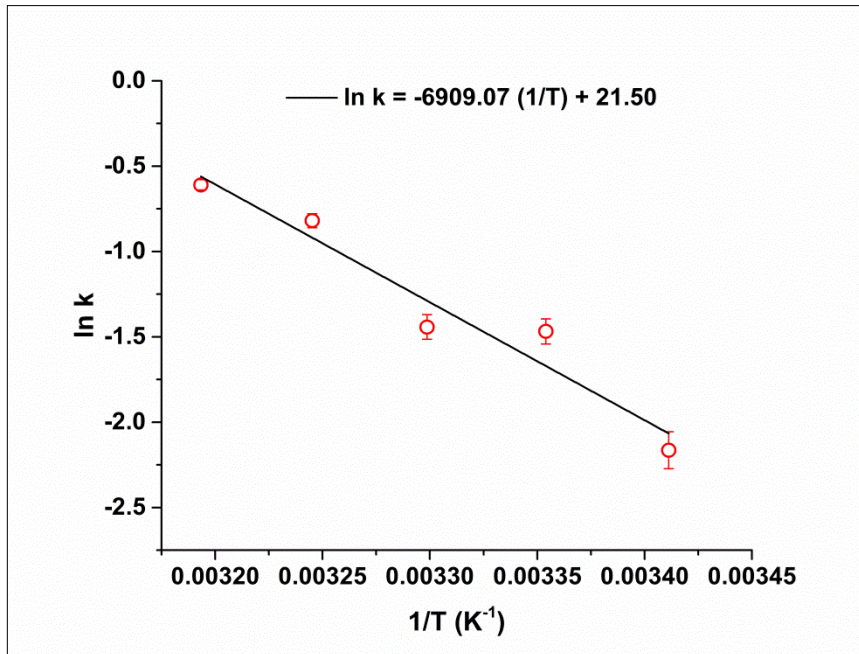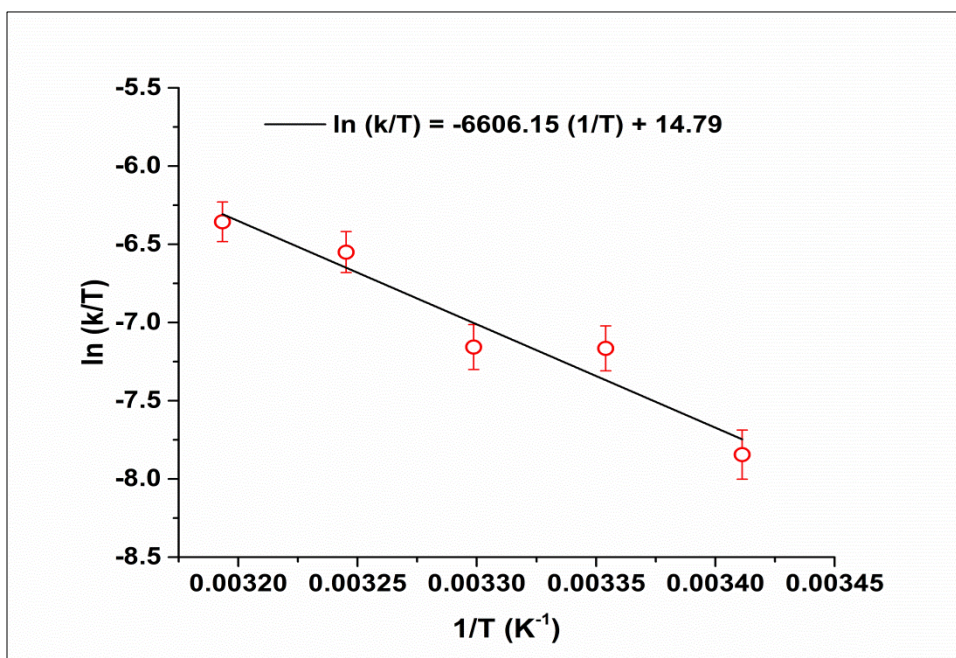

Figure 4.13. The Erying plot, ln (k/T) versus the reciprocal absolute temperature 1/T, for the hydrolysis of ammonia borane catalyzed by ruthenium(0) nanoparticles supported on graphene in the temperature range 20 - 40 °C.

4.4. Catalytic Lifetime of Ruthenium(0) Nanoparticles Supported on Graphene in the Hydrolysis of Ammonia Borane

The catalytic lifetime of ruthenium(0) nanoparticles supported on graphene in the hydrolysis of ammonia-borane was determined by measuring the total turnover number (TTON). Such a catalyst lifetime experiment was performed starting with 0.086 mM ruthenium(0) nanoparticles and 630 mM ammonia borane in 50 mL aqueous solution at 25.0 ± 0.1 °C. When the complete conversion is achieved, more ammonia borane was added and the reaction was continued in this way until no hydrogen gas evolution was observed. It was found that the ruthenium(0) nanoparticles supported on graphene provide 200000 turnovers of hydrogen gas generation from the hydrolysis of ammonia borane over 192 hours before deactivation. This corresponds to a turnover frequency of 149.5 min^{-1}.

The observation that the TOF value decreases as the reaction proceeds indicates the deactivation of ruthenium(0) nanoparticles catalyst (Figure 4.14). The deactivation of Ru(0)/Graphene catalyst can be attributed to a decrease in accessibility of active sites of ruthenium nanoparticles due to the passivation of metal surface by metaborate ions which accumulate in solution as the reaction proceeds.
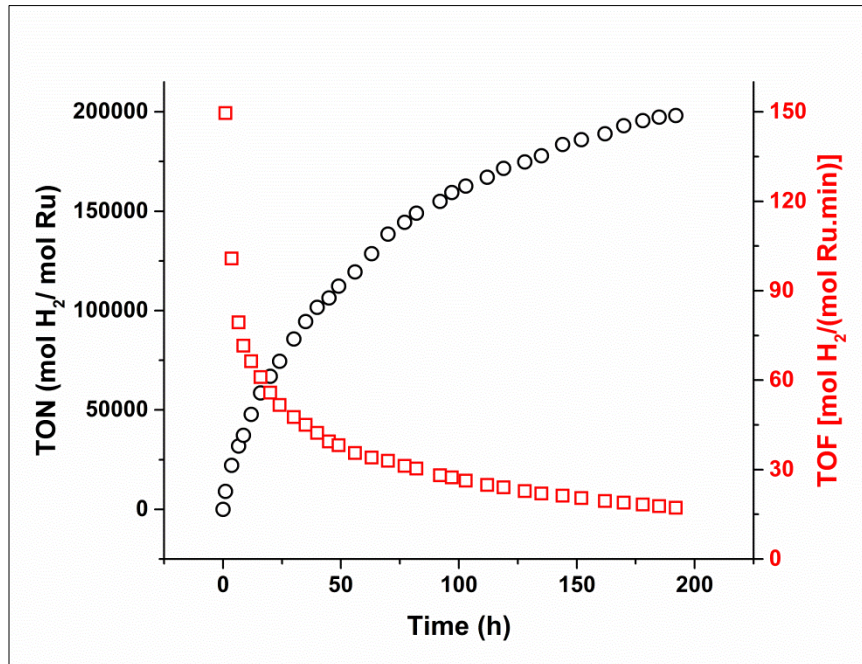
Figure 4.14. The variation in turnover number (TON, in circle) and turnover frequency (TOF, in square) during the catalytic lifetime experiment performed starting with 15 mg Ru(0)/Graphene (ruthenium loading = 1.16% wt Ru, and [Ru] = 0.0861 mM) in 50 mL solution of AB at 25.0 ± 0.1 °C.

Among the ruthenium catalysts for the hydrolytic dehydrogenation of ammonia borane, Ru@Graphene exhibits the highest TTON, exceeding those of Ru(0)@X-NW (TTON = 134100) [142], Ru(0)@HAp (TTON = 87000) [140], Ru(0)NP/PSSA-co-MA (TTON = 51720) [139], Ru(0)@MWCNTs (TTON = 26400) [135], RuNPs@ZK-4 (TTON = 36700) [134], Ru(0)NP/laurate (TTON = 5900) [137]. (Figure 4.15) It should be noted that in the study that uses graphene as a support was missing the lifetime measurements therefore no comparison to this catalyst was possible [22].

68
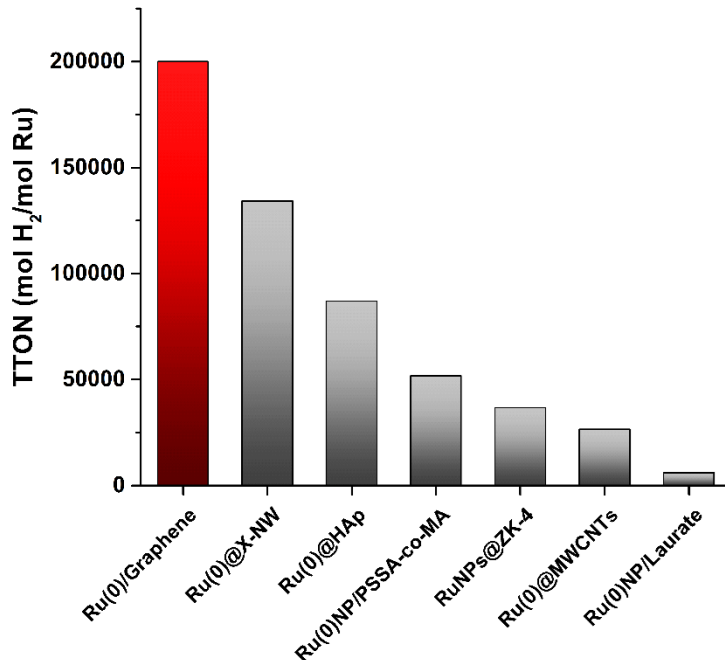
Figure 4.15. Catalytic lifetime of reported ruthenium catalysts (TTON = mol H_2/mol Ru) in the hydrolytic dehydrogenation of ammonia borane [134-142].

TOF values of the reported ruthenium catalysts used in hydrolytic dehydrogenation of ammonia-borane are shown in Figure 4.16. As it can be seen from the comparison of values shown in Figure 4.15, Ru(0)/Graphene having a turnover frequency of 149.5 min^{-1} provided catalytic activity comparable to that of Ru(0)@HAp (TOF = 137 min^{-1}) [140], Ru(0)@X-NW (TOF = 135 min^{-1}) [142], Ru/Carbon (TOF = 113 min^{-1}) [141], RuNPs@ZK-4 (TOF = 90.2 min^{-1}) [134], Ru@Al$_2$O$_3$ (TOF = 83.3 min^{-1}) [138], Ru(0)NP/laurate (TOF = 75 min^{-1}) [137] in hydrolytic dehydrogenation of ammonia borane.

The catalytic activity of Ru(0)/Graphene; however, is lower than that of Ru/C (TOF = 429.5 min^{-1}) [136], Ru(0)@MWCNTs (TOF = 329 min^{-1}) [135], Ru(0)NP/PSSA-co-MA (TOF = 172 min^{-1}) [139]. This significant difference in between the Ru/C and Ru(0)/Graphene catalysts can be attributed to the surface area of the support material, since the carbon black has a larger surface area than that of graphene there will be more ruthenium(0) nanoparticles supported which increases the active sites of the catalyst.

The catalytic activity of Ru(0)/Graphene (TOF = 149.5 min^{-1}) was found to be larger than that of the similar study by Cheng et al. which was calculated as TOF = 100 min^{-1} [22]. Since mean particle sizes of Ru(0)/Graphene catalysts having 1.9 and 1.7 nm (this study and Cheng et al.'s study, respectively) are comparable culprit behind the TOF difference may be the trace amount of manganese in the sample.
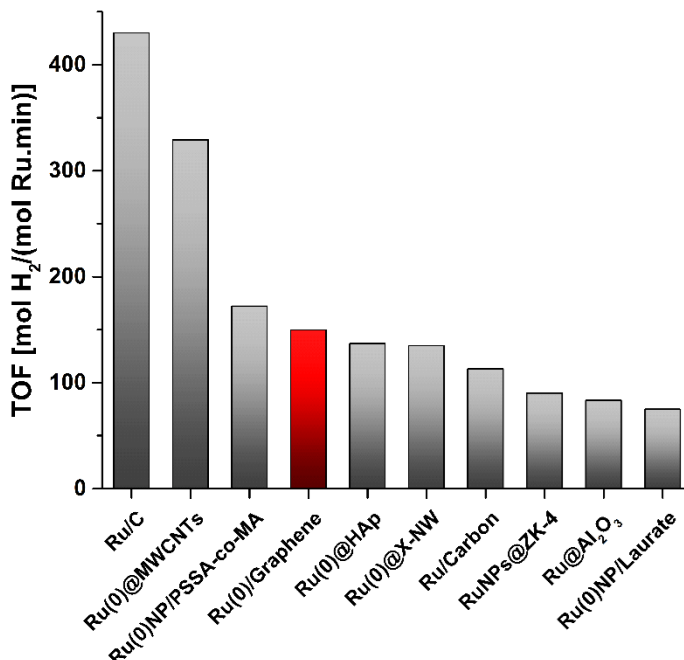
Figure 4.16. Catalytic activity of reported of ruthenium catalysts used for the hydrolysis of ammonia borane [134-142].

4.5. Reusability of Ruthenium(0) Nanoparticles Supported on Graphene Catalyst in the Hydrolysis of Ammonia Borane

Ruthenium(0) nanoparticles supported on graphene were isolated by precipitation followed by drying in vacuum. These isolated ruthenium(0) nanoparticles were redispersed in water and tested for their catalytic activity in the hydrolysis of ammonia borane after being stored for 1 day. After a day of storage, the sample prepared by redispersing the isolated ruthenium(0) nanoparticles was still found to be active catalyst in the hydrolysis of ammonia borane.

The reusability of the catalyst is critical in the practical application. The reaction rates indicate that ruthenium(0) nanoparticles supported on graphene retain 60% of their catalytic activity up to sixth run in the hydrolysis of ammonia borane, when isolated and redispersed in water (Figure 4.17).

Cheng et al. discusses the recyclability of ruthenium(0) nanoparticles supported on graphene up to fourth run for hydrolysis of ammonia borane where the catalysts retain 72% of their initial catalytic activity [22].
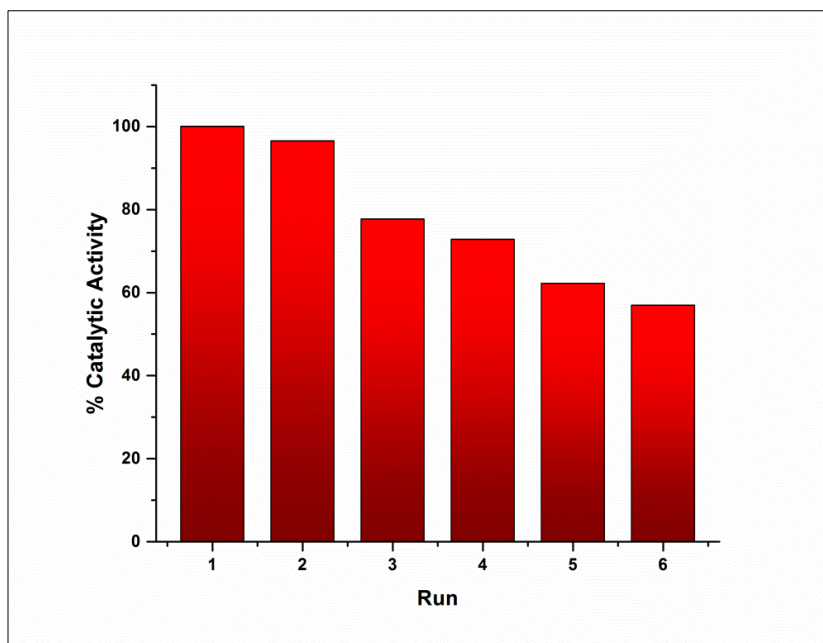
Figure 4.17. The plot of %catalytic activity versus catalytic runs for hydrogen generation from dehydrogenation of AB catalyzed by Ru(0)/Graphene catalyst.

CHAPTER 5

CONCLUSION

This study, covering the synthesis and characterization of ruthenium(0) nanoparticles supported on graphene as catalyst in the hydrolysis of ammonia borane have led to the following conclusions and insights;

- Ruthenium(0) nanoparticles supported on graphene were reproducibly prepared from the reduction of ruthenium(III) ions during the catalytic hydrolysis of AB. Ruthenium(III) ions were impregnated onto graphene oxide from the aqueous solution of ruthenium(III) chloride and then reduced by ammonia borane to ruthenium(0) nanoparticles supported on graphene during its hydrolysis at room temperature.

- Well dispersed ruthenium(0) nanoparticles with an average particle size of 1.9 ± 0.8 nm, supported on graphene, were isolated from the reaction solution by precipitation and characterized by advanced analytical techniques.

- Water-dispersible ruthenium(0) nanoparticles supported on graphene are highly active catalysts in the hydrolysis of ammonia borane even at room temperature.

$$NH_3BH_3(aq) + H_2O(l) \xrightarrow{Ru(0)nanoparticles} NH_4BO_2(aq) + H_2(g) \ (5.1)$$
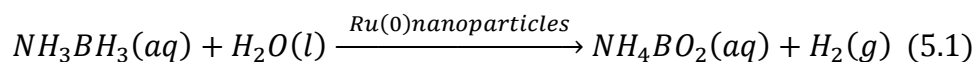
- Ammonia borane can be used as hydrogen storage material since it provides a safe and practical means of producing hydrogen at ambient temperature with water dispersible ruthenium(0) nanoparticles supported on graphene as a catalyst.

- The rate law of the hydrolysis of ammonia borane catalyzed by the ruthenium(0) nanoparticles supported on graphene can be given as;

$$-3\frac{d[NH_3BH_3]}{dt} = \frac{d[H_2]}{dt} = k[Ru] \qquad (5.2)$$

  The catalytic hydrolysis of sodium borohydride is first order with respect to the catalyst concentration and zero order with respect to the substrate concentration.

- The activation energy (E_a), enthalpy of activation ($\Delta H^{\ddagger}$) and entropy of activation ($\Delta S^{\ddagger}$) of ruthenium(0) nanoparticles supported on graphene catalyzed hydrolysis of ammonia borane were found to be 57 ± 1 kJ mol^{-1}, 55 ± 1 kJ mol^{-1} and -75 ± 3 J (mol.K)$^{-1}$, respectively. These values imply on an associative mechanism for the hydrolysis of ammonia borane.

- Ru(0)/Graphene showed high catalytic activity in hydrogen generation from the hydrolysis of AB providing a turnover frequency value up to 149.5 min^{-1} at 25.0 ± 0.1 °C. The high catalytic activity can be attributed to the dispersion of small nanoparticles on the large external surface of graphene layers.

- Ru(0)/Graphene was a long-lived catalyst providing 200000 turnovers in hydrogen generation from the hydrolysis of ammonia borane at 25.0 ± 0.1 °C, over 192 hours before deactivation.

- Ru(0)/Graphene was a reusable catalyst as it provided the complete hydrolysis of AB generating 3 mol H_2 per mole of AB in the sixth run retaining its significant amount of catalytic activity.

- High catalytic activity, reusability, and simple preparation and isolation procedures make Ru(0)/Graphene very attractive catalysts for on-board hydrogen generation from the hydrolysis of ammonia borane.

REFERENCES

[1] Annual Energy Outlook 2014 with Projections to 2040, Retrieved May 31, 2014, from http://www.eia.gov/forecasts/aeo/

[2] Midilli, A.; Ay, M.; Dincer, I.; Rosen, M. A., On hydrogen and hydrogen energy strategies: I: current status and needs. *Renewable and Sustainable Energy Reviews* **2005,** *9* (3), 255-271.

[3] Armaroli, N.; Balzani, V., The Hydrogen Issue. *ChemSusChem* **2011,** *4* (1), 21-36.

[4] Thomas, C. D.; Cameron, A.; Green, R. E.; Bakkenes, M.; Beaumont, L. J.; Collingham, Y. C.; Erasmus, B. F. N.; de Siqueira, M. F.; Grainger, A.; Hannah, L.; Hughes, L.; Huntley, B.; van Jaarsveld, A. S.; Midgley, G. F.; Miles, L.; Ortega-Huerta, M. A.; Townsend Peterson, A.; Phillips, O. L.; Williams, S. E., Extinction risk from climate change. *Nature* **2004,** *427* (6970), 145-148.

[5] Ewan, B. C. R.; Allen, R. W. K., A figure of merit assessment of the routes to hydrogen. *International Journal of Hydrogen Energy* **2005,** *30* (8), 809-819.

[6] Schlapbach, L.; Zuttel, A., Hydrogen-storage materials for mobile applications. *Nature* **2001,** *414* (6861), 353-358.

[7] Züttel,A., Borgschulte, A., Schlapbach, L., *Hydrogen as a Future Energy Carrier*, Wiley-VCH, Weinheim, **2008**.

[8] Züttel, A., Hydrogen storage methods. *Naturwissenschaften* **2004,** *91* (4), 157-172.

[9] Züttel, A., Materials for hydrogen storage. *Materials Today* **2003,** *6* (9), 24-33.

[10] Satyapal, S.; Petrovic, J.; Read, C.; Thomas, G.; Ordaz, G., The U.S. Department of Energy's National Hydrogen Storage Project: Progress towards meeting hydrogen-powered vehicle requirements. *Catalysis Today* **2007,** *120* (3–4), 246-256.

[11] Marder, T. B., Will We Soon Be Fueling our Automobiles with Ammonia–Borane? *Angewandte Chemie International Edition* **2007,** *46* (43), 8116-8118.

[12] Stephens, F. H.; Pons, V.; Tom Baker, R., Ammonia-borane: the hydrogen source par excellence? *Dalton Transactions* **2007,** (25), 2613-2626.

[13] Schlesinger, H. I.; Brown, H. C.; Finholt, A. E.; Gilbreath, J. R.; Hoekstra, H. R.; Hyde, E. K., Sodium Borohydride, Its Hydrolysis and its Use as a Reducing Agent and in the Generation of Hydrogen1. *Journal of the American Chemical Society* **1953,** *75* (1), 215-219.

[14] Kalidindi, S. B.; Indirani, M.; Jagirdar, B. R., First Row Transition Metal Ion-Assisted Ammonia−Borane Hydrolysis for Hydrogen Generation. *Inorganic Chemistry* **2008,** *47* (16), 7424-7429.

[15] Chandra, M.; Xu, Q., A high-performance hydrogen generation system: Transition metal-catalyzed dissociation and hydrolysis of ammonia–borane. *Journal of Power Sources* **2006,** *156* (2), 190-194.

[16] Özkar, S., Chapter 7 - Transition Metal Nanoparticles as Catalyst in Hydrogen Generation from the Boron-Based Hydrogen Storage Materials. In *New and Future Developments in Catalysis*, Suib, S. L., Ed. Elsevier: Amsterdam, 2013; pp 165-189.

[17] Xu, Q.; Chandra, M., Catalytic activities of non-noble metals for hydrogen generation from aqueous ammonia–borane at room temperature. *Journal of Power Sources* **2006,** *163* (1), 364-370.

[18] Chandra, M.; Xu, Q., Dissociation and hydrolysis of ammonia-borane with solid acids and carbon dioxide: An efficient hydrogen generation system. *Journal of Power Sources* **2006,** *159* (2), 855-860.

[19] Chandra, M.; Xu, Q., Room temperature hydrogen generation from aqueous ammonia-borane using noble metal nano-clusters as highly active catalysts. *Journal of Power Sources* **2007,** *168* (1), 135-142.

[20] Aiken Iii, J. D.; Finke, R. G., A review of modern transition-metal nanoclusters: their synthesis, characterization, and applications in catalysis. *Journal of Molecular Catalysis A: Chemical* **1999,** *145* (1–2), 1-44.

[21] "The Nobel Prize in Physics 2010". *Nobelprize.org.* Nobel Media AB 2013. Web. Retrieved 31 May 2014 from
http://www.nobelprize.org/nobel_prizes/physics/laureates/2010/

[22] Cao, N.; Luo, W.; Cheng, G., One-step synthesis of graphene supported Ru nanoparticles as efficient catalysts for hydrolytic dehydrogenation of ammonia borane. *International Journal of Hydrogen Energy* **2013,** *38* (27), 11964-11972.

[23] Turner, J. A., Sustainable Hydrogen Production. *Science* **2004,** *305* (5686), 972-974.

[24] van den Berg, A. W. C.; Arean, C. O., Materials for hydrogen storage: current research trends and perspectives. *Chemical Communications* **2008,** (6), 668-681.

[25] Demirci, U. B.; Miele, P., Chemical hydrogen storage: 'material' gravimetric capacity versus 'system' gravimetric capacity. *Energy & Environmental Science* **2011,** *4* (9), 3334-3341.

[26] Hirscher, M.; Hirose, K., *Handbook of Hydrogen Storage: New Materials for Future Energy Storage*. Wiley: 2010.

[27] Bühl, M.; Steinke, T.; von Ragué Schleyer, P.; Boese, R., Solvation Effects on Geometry and Chemical Shifts. An Ab Initio/IGLO Reconciliation of Apparent Experimental Inconsistencies on H3B · NH3. *Angewandte Chemie International Edition in English* **1991,** *30* (9), 1160-1161.

[28] Klooster, W. T.; Koetzle, T. F.; Siegbahn, P. E. M.; Richardson, T. B.; Crabtree, R. H., Study of the N−H···H−B Dihydrogen Bond Including the Crystal Structure of BH_3NH_3 by Neutron Diffraction. *Journal of the American Chemical Society* **1999,** *121* (27), 6337-6343.

[29] Richardson, T.; de Gala, S.; Crabtree, R. H.; Siegbahn, P. E. M., Unconventional Hydrogen Bonds: Intermolecular B-H···H-N Interactions. *Journal of the American Chemical Society* **1995,** *117* (51), 12875-12876.

[30] Siegbahn, P. E. M.; Eisenstein, O.; Rheingold, A. L.; Koetzle, T. F., A New Intermolecular Interaction: Unconventional Hydrogen Bonds with Element−Hydride Bonds as Proton Acceptor. *Accounts of Chemical Research* **1996,** *29* (7), 348-354.

[31] Haynes, W. M., *CRC Handbook of Chemistry and Physics, 95th Edition*. Taylor & Francis: 2014.

[32] Jaska, C. A.; Temple, K.; Lough, A. J.; Manners, I., Rhodium-catalyzed formation of boron-nitrogen bonds: a mild route to cyclic aminoboranes and borazines. *Chemical Communications* **2001,** (11), 962-963.

[33] Denney, M. C.; Pons, V.; Hebden, T. J.; Heinekey, D. M.; Goldberg, K. I., Efficient Catalysis of Ammonia Borane Dehydrogenation. *Journal of the American Chemical Society* **2006,** *128* (37), 12048-12049.

[34] Baitalow, F.; Baumann, J.; Wolf, G.; Jaenicke-Rößler, K.; Leitner, G., Thermal decomposition of B−N−H compounds investigated by using combined thermoanalytical methods. *Thermochimica Acta* **2002,** *391* (1–2), 159-168.

[35] Wolf, G.; Baumann, J.; Baitalow, F.; Hoffmann, F. P., Calorimetric process monitoring of thermal decomposition of B−N−H compounds. *Thermochimica Acta* **2000,** *343* (1–2), 19-25.

[36] Erdogan, H.; Metin, O.; Ozkar, S., In situ-generated PVP-stabilized palladium(0) nanocluster catalyst in hydrogen generation from the methanolysis of ammonia-borane. *Physical Chemistry Chemical Physics* **2009,** *11* (44), 10519-10525.

[37] Umegaki, T.; Yan, J.-M.; Zhang, X.-B.; Shioyama, H.; Kuriyama, N.; Xu, Q., Boron- and nitrogen-based chemical hydrogen storage materials. *International Journal of Hydrogen Energy* **2009,** *34* (5), 2303-2311.

[38] Kim, J.; University, W. M., *Synthesis, Characterization, and Catalytic Application of Gold Nanoparticles*. Western Michigan University: 2008.

[39] Gibson, K.; Pula, D., Nanoparticles: Environmental risk and regulation. *Environmental Quality Management* **2009,** *18* (3), 1-7.

[40] Shi, J.; Votruba, A. R.; Farokhzad, O. C.; Langer, R., Nanotechnology in Drug Delivery and Tissue Engineering: From Discovery to Applications. *Nano Letters* **2010,** *10* (9), 3223-3230.

[41] Fedlheim, D. L.; Foss, C. A., *Metal Nanoparticles: Synthesis, Characterization, and Applications*. Taylor & Francis: 2001.

[42] Cruz, R. M. S.; Rubilar, J. F.; Khmelinskii, I.; Vieira, M. C., Nanotechnology in Food Applications. In *Advances in Food Science and Technology*, John Wiley & Sons, Inc.: 2013; pp 103-122.

[43] Elghanian, R.; Storhoff, J. J.; Mucic, R. C.; Letsinger, R. L.; Mirkin, C. A., Selective Colorimetric Detection of Polynucleotides Based on the Distance-Dependent Optical Properties of Gold Nanoparticles. *Science* **1997,** *277* (5329), 1078-1081.

[44] Colvin, V. L.; Schlamp, M. C.; Alivisatos, A. P., Light-emitting diodes made from cadmium selenide nanocrystals and a semiconducting polymer. *Nature* **1994,** *370* (6488), 354-357.

[45] Glanz, J., Computer scientists rethink their discipline's foundations. *Science* **1995,** *269* (5229), 1363-1364.

[46] Antonietti, M.; Göltner, C., Superstructures of Functional Colloids: Chemistry on the Nanometer Scale. *Angewandte Chemie International Edition in English* **1997,** *36* (9), 910-928.

[47] Schön, G.; Simon, U., A fascinating new field in colloid science: small ligand-stabilized metal clusters and their possible application in microelectronics. *Colloid Polym Sci* **1995,** *273* (3), 202-218.

[48] Lin, Y.; Finke, R. G., Novel Polyoxoanion- and Bu_4N^+-Stabilized, Isolable, and Redissolvable, 20-30-.ANG. $Ir_{300-900}$ Nanoclusters: The Kinetically Controlled Synthesis, Characterization, and Mechanism of Formation of Organic Solvent-Soluble, Reproducible Size, and Reproducible Catalytic Activity Metal Nanoclusters. *Journal of the American Chemical Society* **1994,** *116* (18), 8335-8353.

[49] Bönnemann, H.; Braun, G. A., Enantioselective Hydrogenations on Platinum Colloids. *Angewandte Chemie International Edition in English* **1996,** *35* (17), 1992-1995.

[50] Stein, J.; Lewis, L. N.; Gao, Y.; Scott, R. A., In Situ Determination of the Active Catalyst in Hydrosilylation Reactions Using Highly Reactive Pt(0) Catalyst Precursors. *Journal of the American Chemical Society* **1999,** *121* (15), 3693-3703.

[51] Wilcoxon, J. P.; Martino, T.; Klavetter, E.; Sylwester, A. P., Synthesis and Catalytic Properties of Metal and Semiconductor Nanoclusters. In *Nanophase Materials*, Hadjipanayis, G.; Siegel, R., Eds. Springer Netherlands: 1994; Vol. 260, pp 771-780.

[52] Schmidt, T. J.; Noeske, M.; Gasteiger, H. A.; Behm, R. J.; Britz, P.; Brijoux, W.; Bönnemann, H., Electrocatalytic Activity of PtRu Alloy Colloids for CO and CO/H_2 Electrooxidation: Stripping Voltammetry and Rotating Disk Measurements. *Langmuir* **1997,** *13* (10), 2591-2595.

[53] Vargaftik, M. N.; Zagorodnikov, V. P.; Stolarov, I. P.; Moiseev, I. I.; Kochubey, D. I.; Likholobov, V. A.; Chuvilin, A. L.; Zamaraev, K. I., Giant palladium clusters as catalysts of oxidative reactions of olefins and alcohols. *Journal of Molecular Catalysis* **1989,** *53* (3), 315-348.

[54] Reetz, M. T.; Quaiser, S. A.; Merk, C., Electrochemical Preparation of Nanostructured Titanium Clusters: Characterization and Use in McMurry-Type Coupling Reactions. *Chemische Berichte* **1996,** *129* (7), 741-743.

[55] Reetz, M. T.; Breinbauer, R.; Wanninger, K., Suzuki and Heck reactions catalyzed by preformed palladium clusters and palladiumnickel bimetallic clusters. *Tetrahedron letters* **1996,** *37* (26), 4499-4502.

[56] Reetz, M. T.; Lohmer, G., Propylene carbonate stabilized nanostructured palladium clusters as catalysts in Heck reactions. *Chemical Communications* **1996,** (16), 1921-1922.

[57] Reetz, M. T.; Breinbauer, R.; Wedemann, P.; Binger, P., Nanostructured nickel-clusters as catalysts in [3+2]cycloaddition reactions. *Tetrahedron* **1998,** *54* (7), 1233-1240.

[58] Sonti, S. V.; Bose, A., Cell Separation Using Protein-A-Coated Magnetic Nanoclusters. *Journal of Colloid and Interface Science* **1995,** *170* (2), 575-585.

[59] Reetz, M. T.; Winter, M.; Dumpich, G.; Lohau, J.; Friedrichowski, S., Fabrication of Metallic and Bimetallic Nanostructures by Electron Beam Induced Metallization of Surfactant Stabilized Pd and Pd/Pt Clusters. *Journal of the American Chemical Society* **1997,** *119* (19), 4539-4540.

[60] Vossmeyer, T.; DeIonno, E.; Heath, J. R., Light-Directed Assembly of Nanoparticles. *Angewandte Chemie International Edition in English* **1997,** *36* (10), 1080-1083.

[61] Schmid, G., *Nanoparticles: From Theory to Application*. Wiley: 2011.

[62] Pool, R., Clusters: Strange Morsels of Matter: When metals or semiconductors are shrunk down to clumps only 10 or 100 atoms in size, they become a "totally new class of materials" with potentially valuable applications. *Science* **1990,** *248* (4960), 1186-1188.

[63] Marquardt, P.; Börngen, L.; Nimtz, G.; Sonnberger, R.; Gleiter, H.; Zhu, J., Microwave absorption by small metal particles. *Physics Letters A* **1986,** *114* (1), 39-42.

[64] Henglein, A., Small-particle research: physicochemical properties of extremely small colloidal metal and semiconductor particles. *Chemical Reviews* **1989,** *89* (8), 1861-1873.

[65] Schön, G.; Simon, U., A fascinating new field in colloid science: small ligand-stabilized metal clusters and their possible application in microelectronics. *Colloid Polym Sci* **1995,** *273* (3), 202-218.

[66] Weller, H.; Eychmüller, A., Preparation and characterization of semiconductor nanoparticles. In *Studies in Surface Science and Catalysis*, Prashant, V. K.; Dan, M., Eds. Elsevier: 1997; Vol. Volume 103, pp 5-22.

[67] Aiken Iii, J. D.; Lin, Y.; Finke, R. G., A perspective on nanocluster catalysis: polyoxoanion and $(n\text{-}C_4H_9)_4N^+$ stabilized $Ir(0)_{\sim300}$ nanocluster 'soluble heterogeneous catalysts'. *Journal of Molecular Catalysis A: Chemical* **1996,** *114* (1–3), 29-51.

[68] Wilcoxon, J. P.; Williamson, R. L.; Baughman, R., Optical properties of gold colloids formed in inverse micelles. *The Journal of Chemical Physics* **1993,** *98* (12), 9933-9950.

[69] Parsapour, F.; Kelley, D. F.; Craft, S.; Wilcoxon, J. P., Electron transfer dynamics in MoS_2 nanoclusters: Normal and inverted behavior. *The Journal of Chemical Physics* **1996,** *104* (13), 4978-4987.

[70] Steigerwald, M. L.; Brus, L. E., Semiconductor crystallites: a class of large molecules. *Accounts of Chemical Research* **1990,** *23* (6), 183-188.

[71] Pocard, N. L.; Alsmeyer, D. C.; McCreery, R. L.; Neenan, T. X.; Callstrom, M. R., Nanoscale platinum(0) clusters in glassy carbon: synthesis, characterization, and uncommon catalytic activity. *Journal of the American Chemical Society* **1992,** *114* (2), 769-771.

[72] Ng Cheong Chan, Y.; Schrock, R. R.; Cohen, R. E., Synthesis of single silver nanoclusters within spherical microdomains in block copolymer films. *Journal of the American Chemical Society* **1992,** *114* (18), 7295-7296.

[73] Zhao, M.; Sun, L.; Crooks, R. M., Preparation of Cu Nanoclusters within Dendrimer Templates. *Journal of the American Chemical Society* **1998,** *120* (19), 4877-4878.

[74] Verwey, E. J. W.; Overbeek, J. T. G.; Overbeek, J. T. G., *Theory of the Stability of Lyophobic Colloids*. Dover Publications: 1999.

[75] Ninham, B. W., On progress in forces since the DLVO theory. *Advances in Colloid and Interface Science* **1999,** *83* (1–3), 1-17.

[76] Özkar, S.; Finke, R. G., Nanocluster Formation and Stabilization Fundamental Studies: Ranking Commonly Employed Anionic Stabilizers via the Development, Then Application, of Five Comparative Criteria. *Journal of the American Chemical Society* **2002,** *124* (20), 5796-5810.

[77] Schmid, G., General Introduction. In *Clusters and Colloids*, Wiley-VCH Verlag GmbH: 2007; 1-4.

[78] Grubbs, R. B., Roles of Polymer Ligands in Nanoparticle Stabilization. *Polymer Reviews* **2007,** *47* (2), 197-215.

[79] Napper, D. H., *Polymeric stabilization of colloidal dispersions*. Academic Press Incorporated: 1983.

[80] Iwasawa, Y., *Tailored Metal Catalysts*. Springer: 1986.

[81] Ruska E., Nobel Lecture: The Development of the Electron Microscope and of Electron Microscopy". *Nobelprize.org.* Nobel Media AB 2014. Retrieved 31 May 2014 from http://www.nobelprize.org/nobel_prizes/physics/laureates/1986/ruska-lecture.html

[82] Reimer, L., *Scanning Electron Microscopy: Physics of Image Formation and Microanalysis.* Springer: 1998.

[83] Skoog, D. A.; Holler, F. J.; Crouch, S. R., *Principles of Instrumental Analysis*. Thomson Brooks/Cole: 2007.

[84] "The Nobel Prize in Physics 1952". *Nobelprize.org.* Nobel Media AB 2014. Retrieved 31 May 2014 from http://www.nobelprize.org/nobel_prizes/physics/laureates/1952/

[85] Binnig, G.; Quate, C.; Gerber, Ch. Atomic Force Microscope. *Physical Review Letter*s, **1986**, *56*, 9, 930-933.

[86] Cooper, G. M.; Hausman, R. E., *The Cell: A Molecular Approach*. ASM Press: 2004.

[87] Lehninger, A. L.; Nelson, D. L.; Cox, M. M., *Lehninger Principles of Biochemistry*. W. H. Freeman: 2005.

[88] Thomas, J. M.; Thomas, W. J., *Principles and Practice of Heterogeneous Catalysis*. Wiley: 1997.

[89] W. Ostwald, *Phys. Z.* **1902,** *3*, 313.

[90] Laidler, K. J. A glossary of terms used in chemical kinetics, including reaction dynamics (IUPAC Recommendations 1996) *Pure and Applied Chemistry* **2009,** *68* (1), 149-192.

[91] Hawkins, S., *Industrial Catalysis: A Practical Approach*. Wiley: 2006.

[92] Arrhenius, S.A. Über die Reaktionsgeschwindigkeit bei der Inversion von Rohrzucker durch Säuren. *J. Phys. Chem.* **1889,** *4*, 226-248.

[93] Eyring, H., The Activated Complex in Chemical Reactions. *The Journal of Chemical Physics* **1935,** *3* (2), 107-115.

[94] Ertl, G., Reactions at Surfaces: From Atoms to Complexity (Nobel Lecture). *Angewandte Chemie International Edition* **2008,** *47* (19), 3524-3535.

[95] Emig, G., Wirkungsweise und Einsatz von Katalysatoren. *Chemie in unserer Zeit* **1987,** *21* (4), 128-137.

[96] Pool, R., Clusters: Strange Morsels of Matter: When metals or semiconductors are shrunk down to clumps only 10 or 100 atoms in size, they become a "totally new class of materials" with potentially valuable applications. *Science* **1990,** *248* (4960), 1186-1188.

[97] Fitzer, E.; Kochling, K.; Boehm, H.; Marsh, H., Recommended terminology for the description of carbon as a solid (IUPAC Recommendations 1995). *Pure and Applied Chemistry* **2009** *67* (3), 375-518.

[98] Geim, A. K.; Novoselov, K. S., The rise of graphene. *Nat Mater* **2007,** *6* (3), 183-191.

[99] Dreyer, D. R.; Park, S.; Bielawski, C. W.; Ruoff, R. S., The chemistry of graphene oxide. *Chemical Society Reviews* **2010,** *39* (1), 228-240.

[100] Schafhaeutl, C., Ueber die Verbindungen des Kohlenstoffes mit Silicium, Eisen und anderen Metallen, welche die verschiedenen Gallungen von Roheisen, Stahl und Schmiedeeisen bilden. *Journal für Praktische Chemie* **1840,** *21* (1), 129-157.

[101] Schafhaeutl, C., LXXXVI. On the combinations of carbon with silicon and iron, and other metals, forming the different species of cast iron, steel, and malleable iron. *Philosophical Magazine Series 3* **1840,** *16* (106), 570-590.

[102] Brodie, B. C., On the Atomic Weight of Graphite. *Philosophical Transactions of the Royal Society of London* **1859,** *149*, 249-259.

[103] Brodie, B. C., XXIII.-Researches on the atomic weight of graphite. *Quarterly Journal of the Chemical Society of London* **1860,** *12* (1), 261-268.

[104] Wallace P. R., The Band Theory of Graphite *Physical Review* **1947**, *71*, 622.

[105] Hummers, W. S.; Offeman, R. E., Preparation of Graphitic Oxide. *Journal of the American Chemical Society* **1958,** *80* (6), 1339-1339.

[106] McClure J. W., Diamagnetism of Graphite *Physical Review* **1956** *104*, 666.

[107] Semenoff G. W., Condensed-Matter Simulation of a Three-Dimensional Anomaly *Physical Review Letters* **1984** *53*, 2449.

[108] IUPAC. *Compendium of Chemical Terminology, 2nd ed.* (the "Gold Book"). Compiled by A.D. McNaught and A. Wilkinson, Blackwell Scientific Publications, Oxford, UK (1997).

[109] Peierls, R. E., Quelques proprietes typiques des corpses solides. *Ann. I. H. Poincare* **1935,** *5*, 177-222.

[110] Landau, L. D., Zur Theorie der phasenumwandlungen II. *Phys. Z. Sowjetunion* **1937,** *11*, 26-35.

[111] Novoselov, K. S.; Geim, A. K.; Morozov, S. V.; Jiang, D.; Zhang, Y.; Dubonos, S. V.; Grigorieva, I. V.; Firsov, A. A., Electric Field Effect in Atomically Thin Carbon Films. *Science* **2004,** *306* (5696), 666-669.

[112] Palermo, V., Not a molecule, not a polymer, not a substrate... the many faces of graphene as a chemical platform. *Chemical Communications* **2013,** *49* (28), 2848-2857.

[113] Stankovich, S.; Dikin, D. A.; Piner, R. D.; Kohlhaas, K. A.; Kleinhammes, A.; Jia, Y.; Wu, Y.; Nguyen, S. T.; Ruoff, R. S., Synthesis of graphene-based nanosheets via chemical reduction of exfoliated graphite oxide. *Carbon* **2007,** *45* (7), 1558-1565.

[114] Yu, Q.; Lian, J.; Siriponglert, S.; Li, H.; Chen, Y. P.; Pei, S.-S., Graphene segregated on Ni surfaces and transferred to insulators. *Applied Physics Letters* **2008,** *93* (11), 113103.

[115] Zhu, M.; Wang, J.; Holloway, B. C.; Outlaw, R. A.; Zhao, X.; Hou, K.; Shutthanandan, V.; Manos, D. M., A mechanism for carbon nanosheet formation. *Carbon* **2007,** *45* (11), 2229-2234.

[116] Horiuchi, S.; Gotou, T.; Fujiwara, M.; Asaka, T.; Yokosawa, T.; Matsui, Y., Single graphene sheet detected in a carbon nanofilm. *Applied Physics Letters* **2004,** *84* (13), 2403-2405.

[117] Wu, Z.-S.; Ren, W.; Gao, L.; Liu, B.; Jiang, C.; Cheng, H.-M., Synthesis of high-quality graphene with a pre-determined number of layers. *Carbon* **2009,** *47* (2), 493-499.

[118] Vázquez de Parga, A. L.; Calleja, F.; Borca, B.; Passeggi, M. C. G.; Hinarejos, J. J.; Guinea, F.; Miranda, R., Periodically Rippled Graphene: Growth and Spatially Resolved Electronic Structure. *Physical Review Letters* **2008,** *100*, 056807

[119] Cano-Márquez, A. G.; Rodríguez-Macías, F. J.; Campos-Delgado, J.; Espinosa-González, C. G.; Tristán-López, F.; Ramírez-González, D.; Cullen, D. A.; Smith, D. J.; Terrones, M.; Vega-Cantú, Y. I., Ex-MWNTs: Graphene Sheets and Ribbons Produced by Lithium Intercalation and Exfoliation of Carbon Nanotubes. *Nano Letters* **2009,** *9* (4), 1527-1533.

[120] Nair, R. R.; Blake, P.; Grigorenko, A. N.; Novoselov, K. S.; Booth, T. J.; Stauber, T.; Peres, N. M. R.; Geim, A. K., Fine Structure Constant Defines Visual Transparency of Graphene. *Science* **2008,** *320* (5881), 1308.

[121] Lee, C.; Wei, X.; Kysar, J. W.; Hone, J., Measurement of the Elastic Properties and Intrinsic Strength of Monolayer Graphene. *Science* **2008,** *321* (5887), 385-388.

[122] Balandin, A. A.; Ghosh, S.; Bao, W.; Calizo, I.; Teweldebrhan, D.; Miao, F.; Lau, C. N., Superior Thermal Conductivity of Single-Layer Graphene. *Nano Letters* **2008,** *8* (3), 902-907.

[123] Murali, R.; Yang, Y.; Brenner, K.; Beck, T.; Meindl, J. D., Breakdown current density of graphene nanoribbons. *Applied Physics Letters* **2009,** *94* (24), 243114.

[124] Chen, J.-H.; Jang, C.; Xiao, S.; Ishigami, M.; Fuhrer, M. S., Intrinsic and extrinsic performance limits of graphene devices on SiO2. *Nat Nano* **2008,** *3* (4), 206-209.

[125] Bolotin, K. I.; Sikes, K. J.; Jiang, Z.; Klima, M.; Fudenberg, G.; Hone, J.; Kim, P.; Stormer, H. L., Ultrahigh electron mobility in suspended graphene. *Solid State Communications* **2008,** *146* (9–10), 351-355.

[126] Bao, W.; Miao, F.; Chen, Z.; Zhang, H.; Jang, W.; Dames, C.; Lau, C. N., Controlled ripple texturing of suspended graphene and ultrathin graphite membranes. *Nat Nano* **2009,** *4* (9), 562-566.

[127] Yoon, D.; Son, Y.-W.; Cheong, H., Negative Thermal Expansion Coefficient of Graphene Measured by Raman Spectroscopy. *Nano Letters* **2011,** *11* (8), 3227-3231.

[128] Geim, A. K., Graphene: Status and Prospects. *Science* **2009,** *324* (5934), 1530-1534.

[129] Liu, L.; Ryu, S.; Tomasik, M. R.; Stolyarova, E.; Jung, N.; Hybertsen, M. S.; Steigerwald, M. L.; Brus, L. E.; Flynn, G. W., Graphene Oxidation: Thickness-Dependent Etching and Strong Chemical Doping. *Nano Letters* **2008,** *8* (7), 1965-1970.

[130] Zhou, W.; Zhu, J.; Cheng, C.; Liu, J.; Yang, H.; Cong, C.; Guan, C.; Jia, X.; Fan, H. J.; Yan, Q.; Li, C. M.; Yu, T., A general strategy toward graphene@metal oxide core-shell nanostructures for high-performance lithium storage. *Energy & Environmental Science* **2011,** *4* (12), 4954-4961.

[131] Cullity, B. D.; Stock, S. R., *Elements of X-ray Diffraction*. Prentice Hall: 2001.

[132] Goldstein, J.; Newbury, D. E.; Joy, D. C.; Lyman, C. E.; Echlin, P.; Lifshin, E.; Sawyer, L.; Michael, J. R., *Scanning Electron Microscopy and X-ray Microanalysis: Third Edition*. Springer US: 2013.

[133] Woehrle, G. H.; Hutchison, J. E.; Ozkar, S.; Finke, R. G., Analysis of nanoparticle Transmission Electron Microscopy data using a public-domain image-processing program, Image. *Turk. J. Chem.* **2006,** *30* (1), 1-13.

[134] Zahmakiran, M., Preparation and characterization of LTA-type zeolite framework dispersed ruthenium nanoparticles and their catalytic application in the hydrolytic dehydrogenation of ammonia–borane for efficient hydrogen generation. *Materials Science and Engineering: B* **2012,** *177* (8), 606-613.

[135] Akbayrak, S.; Özkar, S., Ruthenium(0) Nanoparticles Supported on Multiwalled Carbon Nanotube As Highly Active Catalyst for Hydrogen Generation from Ammonia–Borane. *ACS Applied Materials & Interfaces* **2012,** *4* (11), 6302-6310.

[136] Liang, H.; Chen, G.; Desinan, S.; Rosei, R.; Rosei, F.; Ma, D., In situ facile synthesis of ruthenium nanocluster catalyst supported on carbon black for hydrogen generation from the hydrolysis of ammonia-borane. *International Journal of Hydrogen Energy* **2012,** *37* (23), 17921-17927.

[137] Durap, F.; Zahmakıran, M.; Özkar, S., Water soluble laurate-stabilized ruthenium(0) nanoclusters catalyst for hydrogen generation from the hydrolysis of ammonia-borane: High activity and long lifetime. *International Journal of Hydrogen Energy* **2009,** *34* (17), 7223-7230.

[138] Can, H.; Metin, Ö., A facile synthesis of nearly monodisperse ruthenium nanoparticles and their catalysis in the hydrolytic dehydrogenation of ammonia borane for chemical hydrogen storage. *Applied Catalysis B: Environmental* **2012,** *125* (0), 304-310.

[139] Metin, Ö.; Şahin, Ş.; Özkar, S., Water-soluble poly(4-styrenesulfonic acid-co-maleic acid) stabilized ruthenium(0) and palladium(0) nanoclusters as highly active catalysts in hydrogen generation from the hydrolysis of ammonia–borane. *International Journal of Hydrogen Energy* **2009,** *34* (15), 6304-6313.

[140] Akbayrak, S.; Erdek, P.; Özkar, S., Hydroxyapatite supported ruthenium(0) nanoparticles catalyst in hydrolytic dehydrogenation of ammonia borane: Insight to the nanoparticles formation and hydrogen evolution kinetics. *Applied Catalysis B: Environmental* **2013,** *142–143* (0), 187-195.

[141] Basu, S.; Brockman, A.; Gagare, P.; Zheng, Y.; Ramachandran, P. V.; Delgass, W. N.; Gore, J. P., Chemical kinetics of Ru-catalyzed ammonia borane hydrolysis. *Journal of Power Sources* **2009,** *188* (1), 238-243.

[142] Akbayrak, S.; Ozkar, S., Ruthenium(0) nanoparticles supported on xonotlite nanowire: a long-lived catalyst for hydrolytic dehydrogenation of ammonia-borane. *Dalton Transactions* **2014,** *43* (4), 1797-1805.

[143] D'Ulivo, A.; Dĕdina, J.; Mester, Z.; Sturgeon, R. E.; Wang Q.; Welz, B., Mechanisms of chemical generation of volatile hydrides for trace element determination (IUPAC Technical Report). *Pure Appl. Chem.,* **2011**, *83*, 6, 1283-1340.